Check for updates

Advancements in silicon carbide-based supercapacitors: materials, performance, and emerging applications

Yangwen Liu,[a] Guanghuan Li,[a] Li Huan*[b] and Sheng Cao [ID] *[c]

Silicon carbide (SiC) nanomaterials have emerged as promising candidates for supercapacitor electrodes due to their unique properties, which encompass a broad electrochemical stability range, exceptional mechanical strength, and resistance to extreme conditions. This review offers a comprehensive overview of the latest advancements in SiC nanomaterials for supercapacitors. It encompasses diverse synthesis methods for SiC nanomaterials, including solid-state, gas-phase, and liquid-phase synthesis techniques, while also discussing the advantages and challenges associated with each method. Furthermore, this review places a particular emphasis on the electrochemical performance of SiC-based supercapacitors, highlighting the pivotal role of SiC nanostructures and porous architectures in enhancing specific capacitance and cycling stability. A deep dive into SiC-based composite materials, such as SiC/carbon composites and SiC/metal oxide hybrids, is also included, showcasing their potential to elevate energy density and cycling stability. Finally, the paper outlines prospective research directions aimed at surmounting existing challenges and fully harnessing SiC's potential in the development of next-generation supercapacitors.

1 Introduction

Supercapacitors, emerging as a novel class of energy storage device, have garnered substantial attention owing to their dis-

[a]School of Materials Sciences and Technology, Guangdong University of Petrochemical Technology, Maoming, 525000, China
[b]Department of Library, Guangdong University of Petrochemical Technology, Maoming, 525000, China. E-mail: huangli@gdupt.edu.cn
[c]School of Physical Science and Technology, State Key Laboratory of Featured Metal Materials and Life-cycle Safety for Composite Structures, Guangxi University, Nanning 530004, China. E-mail: caosheng@gxu.edu.cn

tinctive attributes.[1,2] They offer solutions to modern energy challenges, including higher power density, longer cycle life, rapid charge–discharge rates, low maintenance costs, environmental sustainability, and versatility across a wide temperature range.[3,4] This position supercapacitors as a potential game-changer in energy storage across various domains. One promising application of supercapacitors lies within the electric vehicle sector, where they can complement traditional batteries.[5–8] By doing so, they improve vehicle acceleration performance, enhance range, optimize energy efficiency, and reduce fuel consumption.[9–11] In renewable energy, particularly solar and wind power generation, supercapacitors can effec-

Yangwen Liu is a lecturer at Guangdong University of Petrochemical Technology. He received his PhD from the University of Science and Technology Beijing in 2019. His research involves the synthesis and application of inorganic semiconductor nanomaterials and carbon materials, particularly supercapacitors and photocatalysis.

Yangwen Liu

Sheng Cao is an Associate Professor at Guangxi University. He earned his Ph.D. from the University of Science and Technology Beijing in 2016 and subsequently held the position of Research Fellow at the National University of Singapore from 2017 to 2018. His research focuses on colloidal nanocrystals and their utilization in the development of light-emitting diodes and electrochromic devices.

Sheng Cao

tively store surplus energy and balance supply-demand fluctuations.[12–15] In the smart grid context, supercapacitors can act as energy buffers, stabilizing power supply and promoting grid resilience.[16–19] In essence, supercapacitors offer a sustainable approach to energy storage, reducing carbon footprints and fostering a greener future.[20–22]

It is essential to acknowledge, however, that like any technology, supercapacitors have limitations. Four key limitations warrant attention:[23–28] (a) *Lower energy density*. Supercapacitors typically exhibit lower energy density compared to traditional battery technologies, which remains a significant challenge in the field.[29] Bridging the gap between supercapacitor energy density and practical requirements remains a central focus of supercapacitor research. (b) *Self-discharge*. Supercapacitors suffer from self-discharge, a phenomenon wherein stored energy dissipates over time at a higher rate compared to batteries. (c) *Temperature sensitivity*. Supercapacitors are sensitive to temperature variations, leading to fluctuations in their electrical performance. Extreme temperatures can result in reduced capacitance and increased internal resistance, thereby impacting overall energy storage efficiency. Mitigating this limitation may necessitate additional thermal management systems, introducing complexity and cost considerations. (d) *Cycle stability*. The cycle stability of supercapacitors is influenced by multiple factors, including the type of electrode material. Carbon materials, known for their high cycle stability, are commonly used as electrode materials for electric double-layer capacitors. In contrast, metal compounds and conductive polymers, exhibiting pseudo-capacitance or battery-like behavior, often exhibit weaker cycle stability.

Supercapacitors consist of four main components: electrodes, current collectors, electrolytes, and separators. Among these, electrode materials play a pivotal role in determining SC performance and production costs.[30–32] Thus, a key strategy for overcoming supercapacitor limitations lies in the research and development of high-performance, low-cost electrode materials. Currently, the most widely researched electrode materials for supercapacitors encompass carbon materials,[33,34] metal oxides (or hydroxides),[35–37] and conductive polymers.[38–40] Carbon materials primarily include activated carbon, carbon nanotubes, and graphene, each of which presents unique challenges in controlling the pore size and low utilization of specific surface area, scalable production, high costs, respectively.[41–44] Despite the favorable specific capacitance exhibited by (or hydroxides) and conductive polymers, their conductivity and structural stability are comparatively inadequate, thereby constraining their utility in supercapacitors.[40,45–47] Hence, there arises a need to cultivate an enhanced electrode material, which can surmount the imperfections of supercapacitors.

Currently, there is a growing interest in nanoscale silicon carbide (SiC) as a potential solution to enhance energy storage and power density[48,49] This interest arises from its unique physical and chemical properties, which include high temperature resistance, good mechanical strength, and excellent chemical stability compared to traditional carbon-based materials. In the field of supercapacitors, the advantages of SiC are particularly prominent. Firstly, SiC can remain stable up to 1600 °C, enabling it to operate stably even under extreme conditions.[50] This is particularly beneficial in high-temperature and harsh environments where temperature fluctuations are common, such as in electric vehicles or industrial processes. Secondly, SiC's excellent mechanical properties provide exceptional toughness and wear resistance, making it a robust material for use in harsh environments. Thirdly, SiC's chemical stability ensures long-term performance and durability in various environments, making it a reliable material for supercapacitor applications. Moreover, SiC's good electrical conductivity and tailorable pore structure allow for efficient charge–discharge processes, leading to improved specific capacitance and rate capability. The tunable pore structure of SiC results in a large electrochemical reaction surface and short ion diffusion paths, further enhancing its performance as a supercapacitor material.[47,51] Furthermore, SiC's excellent cycling stability, even under high current densities, makes it as a potential candidate for supercapacitors used in electric vehicles or other demanding applications. Finally, SiC's semiconductor properties enable integration with other electronic components;[52–54] SiC-based supercapacitors offer the promise of improved energy storage, higher energy density, and enhanced durability, making them an enticing choice for a spectrum of applications, including electric vehicles, renewable energy storage, and portable electronics.[55–57]

Given their potential to address specific energy storage requirements, this comprehensive review aims to analyze recent advancements in SiC-based supercapacitors, exploring their material design, fabrication methods, and electrochemical performance. The subsequent sections will provide an in-depth overview of SiC's physical and chemical properties, methods of SiC nanomaterial preparation, and recent developments in SiC-based supercapacitors, emphasizing their applications and breakthroughs in the field.

2 Crystallographic structures and properties

The initial appeal of SiC arises from its exceptional wear resistance and hardness, boasting a Moss hardness rating of 9.2–9.5, surpassed only by carbonized diamond and cubic nitriding shed.[58] The initial application of SiC was in the field of abrasives, followed by its widespread adoption across various industries (see Fig. 1). Furthermore, due to its high thermal conductivity and excellent thermal stability, SiC has also been utilized in refractory materials.[59] Its small thermal expansion coefficient and low thermal stress make it suitable for high-frequency high-power devices and high-temperature electronics.[60] Additionally, the synthesis of SiC typically involves the reaction between silicon and carbon under high temperatures. The resulting SiC components exhibit exceptional radiation resistance, ensuring reliable functionality even when exposed to high-energy cosmic rays.[61] This characteristic
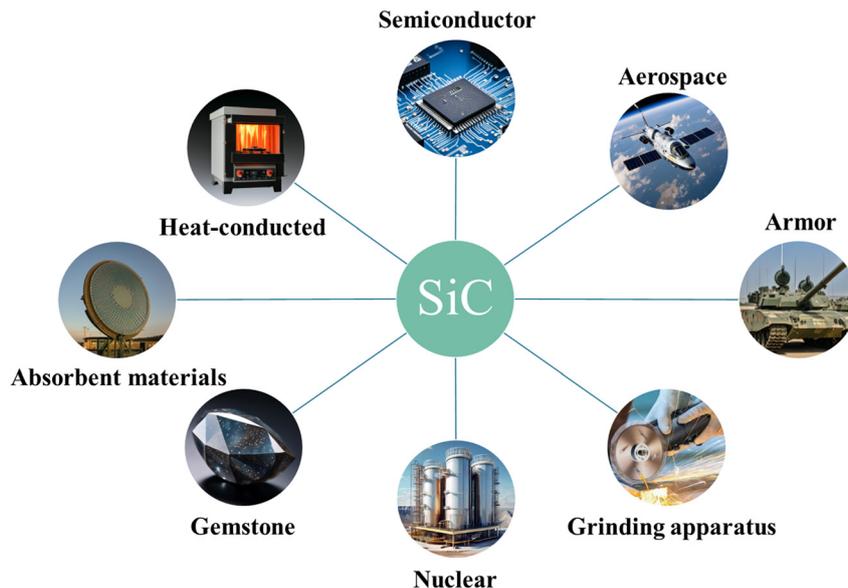
Fig. 1 The utilization of SiC in various fields.

makes them particularly advantageous for applications in space exploration, aerospace engineering, and nuclear energy instrumentation. The chemical properties of SiC are primarily demonstrated by its exceptional chemical stability.[62] For instance, SiC exhibits remarkable resistance to extreme conditions such as high temperatures, strong acids, and strong alkalis.[61] Such a feature holds significant advantages for the use of SiC in catalysis and catalyst support.[63] In this section, we will provide a concise overview of the structure and nanoscale properties of SiC.

3 Crystallographic structures of SiC

SiC is a non-metallic carbide compound formed by covalent bonding between C and Si atoms, both of which belong to Group IV of the periodic table, allowing only a rigid stoichiometry ($Si:C = 1:1$). It is the only stable compound among them, and the earth's crust has abundant reserves of Si and C elements.[63] As shown in Fig. 2i, similar to diamond, SiC has a tetrahedral crystallographic structure. In any of its crystal forms, each C atom is closely surrounded by four Si atoms,
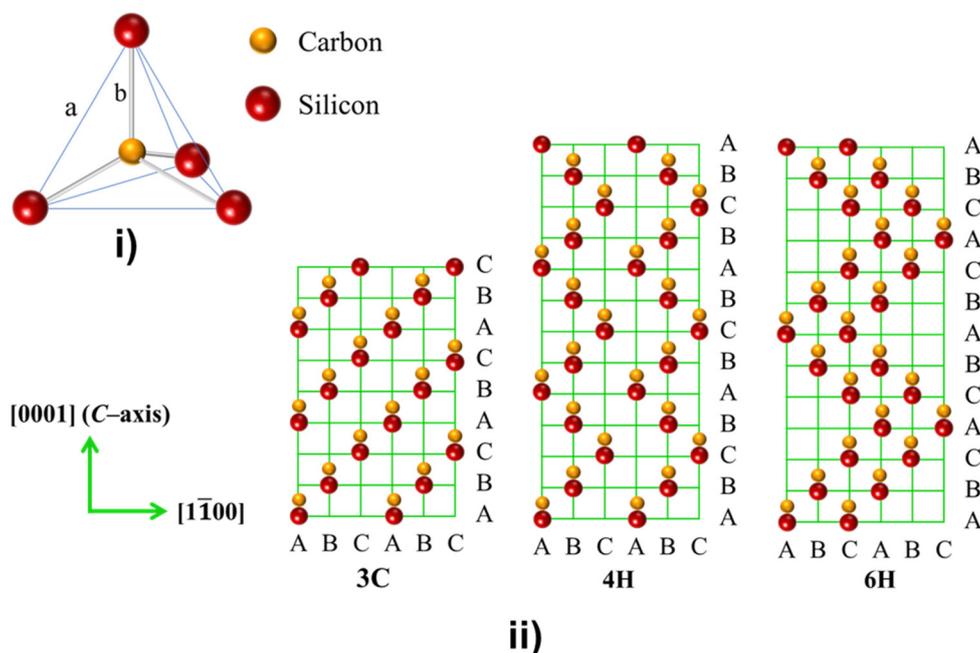

Fig. 2 (i) The fundamental crystal structure of SiC; (ii) sequences of double-layer stacking of 3C-, 4H-, and 6H-SiC.

and *vice versa*, each Si atom is tightly surrounded by four C atoms, interconnected by directed and strong sp³ bonds. The center distance between two nearest neighboring atoms in SiC is 0.189 nm (mark b in Fig. 2i). It is precisely because of this unique crystal structure that SiC possesses advantages such as high temperature resistance, high mechanical strength, high thermal conductivity, high hardness, and chemical stability, which makes SiC-based supercapacitors suitable for harsh environments and high temperatures.[50,64,65]

Despite its robust tetrahedral bonds, SiC exhibits different stacking sequences of C/Si double layers (see Fig. 2ii). This variation arises from the low slip barrier between close-packed staking. Consequently, one of the most distinguishing features of SiC in its crystal structure is the presence of various polytypes. Remarkably, over 250 polytypes have been identified.[61,65] Among these, the cubic close-packed 3C-SiC and the hexagonal close-packed 4H, 6H-SiC (α-SiC) are the most common polymorphic forms. These SiC polytypes possess identical chemical properties but exhibit significant differences in physical characteristics, particularly in optical and electrical performance, including variances in their bandgap.[62,66] This inherent polymorphism enables the straightforward construction of heterogeneous structures *via in situ* self-generation of polymorphic SiC.[51,67] These heterostructures can establish junctions at interfaces, facilitating efficient charge transport and promoting favorable surface reaction kinetics. Consequently, this has the potential to significant enhance the capacitance in SC applications.[51,68,69]

4   Properties of nanoscale SiC

Nanoscale SiC, as the name suggests, is characterized by its nanoscale dimensions, typically ranging from 1 to 100 nanometers. This nanoscale morphology imparts exceptional properties to SiC, including enhanced surface area, quantum confinement effects, and improved mechanical, electrical, and thermal properties.[65,70] The unique characteristics of nanoscale SiC include: (a) *Elevated hardness and strength*. Nano silicon carbide (β-SiC) exhibits superior hardness and strength compared to conventional materials, thereby endowing it with superb wear resistance and corrosion resistance in high temperature, high pressure and severe environments. (b) *Rampant specific surface area*. Given the existing nano-scale silicon carbide fibers, nano SiC possesses a substantial specific surface area, contributing to more adsorption surfaces and augmenting the adsorption capacity. (c) *Porous structure*. Nano SiC possesses a porous structure, the pore size of which can be adjusted. This porosity enhances the material's adsorption capacity as well as adsorption rate. (d) *Exemplary electrical properties*. Nano SiC exhibits remarkable electrical properties, encompassing high breakdown electric field strength, elevated thermal conductivity and unmatched chemical stability. (e) *Superior thermal conductivity*. SiC is a distinguished thermal conductivity material. Nano SiC inherits this attribute, thus presenting significant potential in the field of thermal man-

agement. (f) *Biocompatibility*. Nano SiC demonstrates commendable biocompatibility, rendering it an attractive material in the biomedical sector.

SiC nanomaterials also show outstanding performance in SiC based supercapacitors. SiC nanomaterials have a high specific surface area, which facilitates increased contact with surrounding materials, leading to improved interfacial properties and better adhesion.[71] Moreover, their reduced size allows for efficient dispersion in various matrices, enabling the development of high-performance nanocomposites. Therefore, by manipulating the size, structure, and composition of SiC electrodes at the nanometer scale, higher electrical conductivity, specific surface area, cycling stability, and lifetime can be achieved, with the potential to significantly improve the performance of SiC-based supercapacitors.[48,61] Due to the extensive examination of various structural characteristics of SiC in influential research papers, scholarly books, and comprehensive review articles in recent years, a comprehensive analysis of these factors is beyond the scope of this current contribution, and no further details are provided here.

5   Synthesis of SiC nanomaterials

SiC finds wide applications in fields like chemistry, physics, and biology due to its remarkable chemical properties, physical stability, and biocompatibility.[63,65] Therefore, a vital aspect of applied research centers on synthesizing SiC nanoscale materials. Currently, through the continuous efforts of researchers, numerous technical methods have emerged for the preparation of SiC nanomaterials. In this paper, we categorize the preparation methods of SiC nanomaterials into three main categories based on the states of reactants, phase transitions during the reaction process, and the states of products: solid-phase, vapor-phase, and liquid-phase synthesis methods (see Fig. 3). This section offers a concise overview of these preparation methods, including their formation mechanism and advancements. Additionally, we cite relevant literature to underscore the current state of research in this field.

5.1   Solid-phase synthesis method

Solid-phase synthesis involves the direct reaction of precursor materials containing silicon and carbon source under controlled temperature and pressure conditions. The reaction is generally performed at high temperatures, to facilitate the diffusion of Si and C atom, leading to SiC formation. Solid-state synthesis holds promise for production of porous SiC nanomaterials and offers advantages such as simplicity, scalability, and control over the final product properties. Further research is warranted to optimize the synthesis conditions, enhance yield, and explore novel applications of SiC nanomaterials across various disciplines. Method for solid-phase synthesis SiC nanomaterials include electrospinning, sol–gel, and template method.

5.1.1   Electrospinning. Electrospinning is a versatile and widely employed technique for fabricating nanofibers and
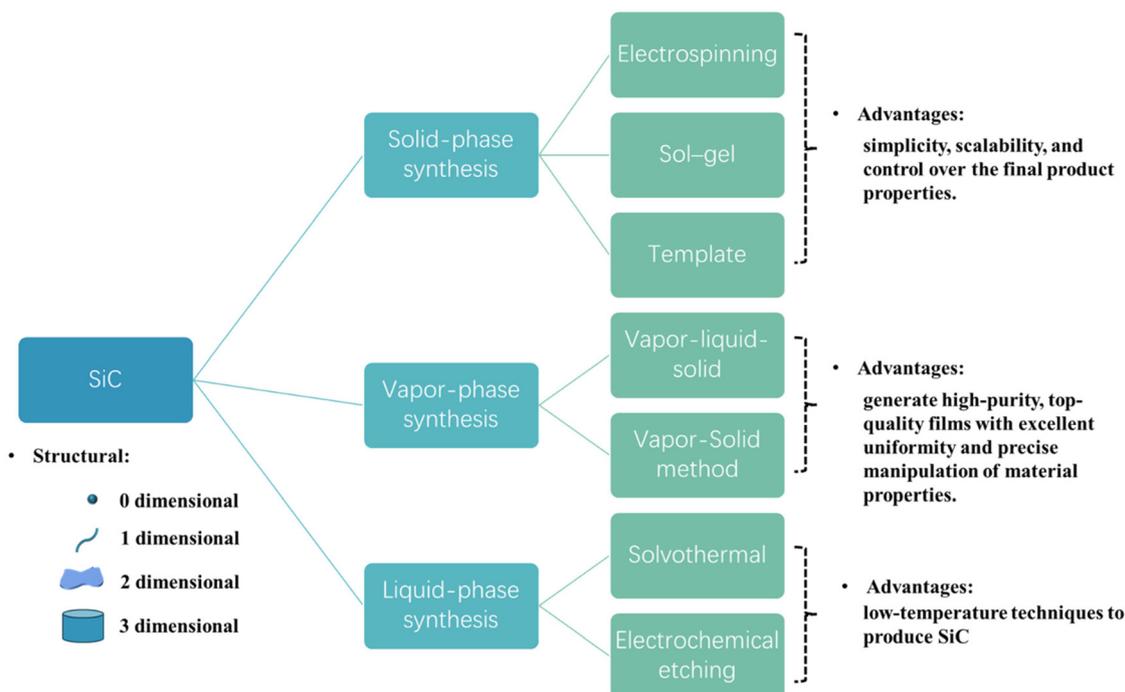
Fig. 3 The strategy for synthesizing SiC nanomaterials.

nanostructured materials.[72,73] Fig. 4a illustrates that an electrospinning setup typically consists of a high-voltage power supply, a syringe pump for controlling the polymer flow rate, and a collector. It involves applying an electric field to draw a charged polymer solution or melt into a fine jet, which then solidifies to form ultrafine fibers with diameters ranging from tens of nanometers to several micrometers.[74–76] The electrospinning process can be controlled to produce continuous fibers, non-woven mats, porous spherical forms or aligned fiber arrays (see Fig. 4b–e), depending on specific application requirements.

One significant advantage of electrospinning lies in its ability to prepare fibers with a porous structure. For example, Kim's research group successfully synthesized SiC fibers by electrospinning technology. They carried out electrospinning of polycarbosilane (PCS) solution at 20 kV and thermally cured the electrospun fibers, resulting in 1 to 3 μm SiC fiber.[77] Our group, on the other hand, achieved mesoporous 3C-SiC hollow fibers (Fig. 4b). These fibers featured completely mesoporous walls, uniform diameter, and high purity in morphology. This accomplishment was realized through single-spinneret electrospinning of a polyureasilazane (PSN) and polyvinylpyrrolidone (PVP) solution, followed by high-temperature pyrolysis treatment.[78] Additionally, Wang *et al.* employed a straightforward approach to fabricate well-aligned SiC nanofibers (Fig. 4c) through the carbothermal reduction of electrospun polyacrylonitrile (PAN) nanofibers and silicon powder.[79] Furthermore, Wei *et al.* the successful synthesis of a flexible ultra-long SiC NWs membrane (Fig. 4d) *via* electrospinning and subsequent high-temperature sintering, using phenolic resin and silica sol

as precursors. System characterization revealed that SiC NWs had a smooth and uniform surface with a diameter distribution primarily ranging from 50–300 nm and a length exceeding tens of micrometers, forming a network structure.[80] Electrospinning proves to be a promising and powerful technique for fabricating nanostructured materials,[81,82] offering unique advantages such as high surface area,[83] morphology control,[84] composition flexibility,[83,85] and scalability.[86,87] However, electrospinning also has some disadvantages: first, the composition of the electrospun materials is limited by the solubility of the components in the spinning solution, which can restrict the preparation of certain complex materials; second, electrospinning requires the spinning solution to have good electrical conductivity, limiting the choice of materials that can be used. Third, the diameter of the electrospun fibers is relatively challenging to control, making it difficult to produce fibers with diameters below a few nanometers. Finally, electrospun materials often require post-treatment steps such as calcination or chemical vapor deposition to obtain the desired properties. These additional steps can increase the complexity and cost of the overall process.

5.1.2 Sol–gel method. The sol–gel method is a versatile technique for producing SiC nanomaterials with precise control over their properties. This method involves a series of chemical reactions that transform a liquid "sol" into a solid "gel". When it comes to SiC nanomaterials, as illustrated in Fig. 5, a sol is created by dissolving silicon sources, such as tetraethoxysilane (TEOS) or silicon alkoxides, and carbon sources, such as furfuryl alcohol or phenolic resin, in a suitable solvent.[90] The precursor solution is then allowed to age,
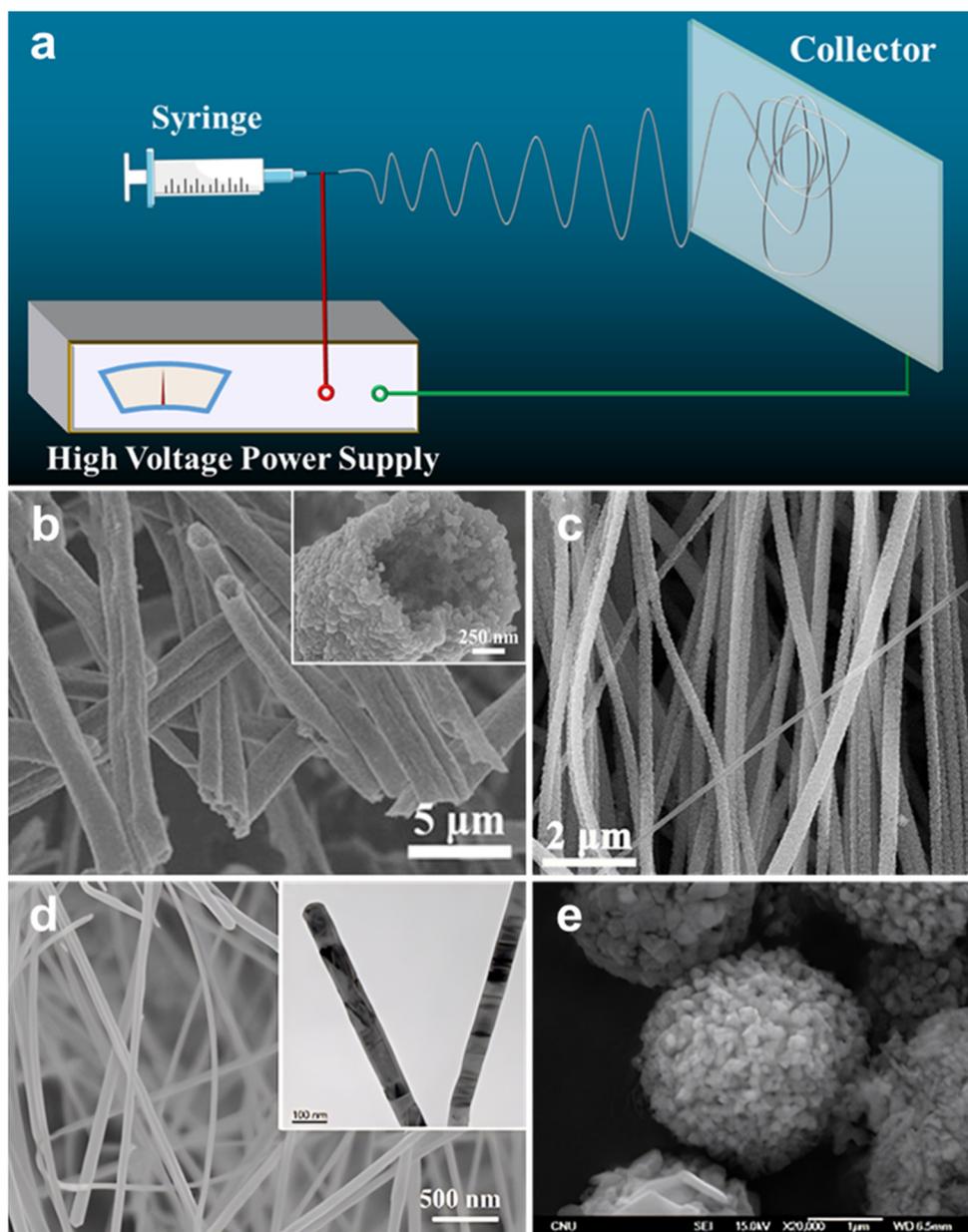
Fig. 4 (a) Schematic diagram of electrospinning. (b) SEM image of mesporous SiC hollow fibers. Reprinted with permission from ref. 78. Copyright 2017 by Nature Publishing Group; (c) SEM image of aligned SiC nanofibers. Reprinted with permission from ref. 79. Copyright 2017 by Elsevier and Copyright Clearance Center; (d) SEM image of SiC nanowires, with the inset showing the TEM image of nanostructure. Reprinted with permission from ref. 88. Copyright 2020 by John Wiley and Sons; (e) SEM image of nanocrystalline porous SiC spherical forms. Reprinted with permission from ref. 89. Copyright 2010 by Elsevier and Copyright Clearance Center.

leading to gel formation, which is subsequently dried and calcined to obtain the desired SiC nanomaterials.[91,92]

One of the key advantages of the sol–gel method lies in its ability to precisely control the properties of SiC nanomaterials. Firstly, the selection of precursors and solvent allows for tailoring the composition and stoichiometry of the final nanomaterials.[93,94] Moreover, the choice of solvent can influence particle size and morphology by regulating the rate of nucleation and growth during gel formation. Additionally, the introduction of surfactants or modifying agents can be employed to finely adjust the size, surface area, and porosity of the resulting SiC nanomaterials.[95,96]

The sol–gel technique facilitates the production of materials with diverse morphologies and structures. For instance, Guo *et al.* devised a modified sol–gel method for preparation of mesoporous silicon carbide, which involved the use of TEOS and phenolic resin to create a binary carbonaceous silicon xerogel. In this process, nickel nitrate was applied as a pore-adjusting reagent during the sol–gel process.[98] The resulting SiC exhibited a surface area of 112 m^2
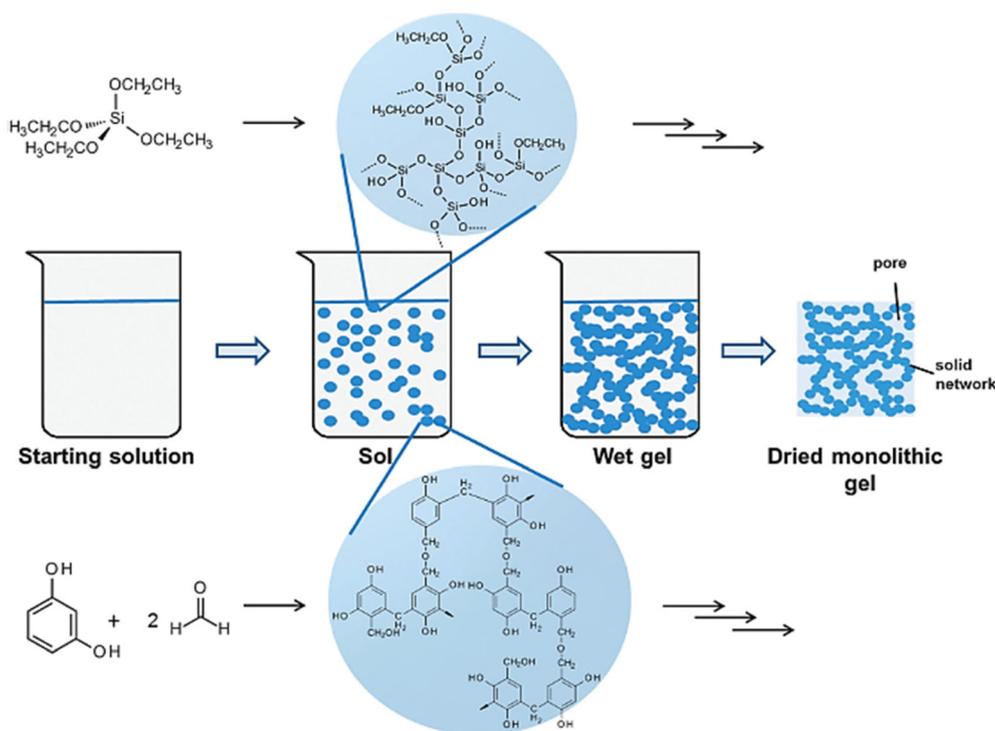
Fig. 5 Schematic representation of the sol–gel process. Reprinted with permission from ref. 97. Copyright 2016 by Royal Society of Chemistry.

g^{-1} (BET) and an average pore diameter of about 10 nm *via* the carbothermal reduction of the binary xerogel. In the same year, Guo's group introduced a novel ternary sol–gel route for synthesizing SiC nanowires (SiC_{nws}) with diameters of about 15 nm and lengths of several μm.[99] Additionally, Fan *et al.* reported the synthesis of monolithic SiC aerogel by carbothermal reduction of RF/SiO$_2$ aerogel, which was prepared using the sol–gel method. The resulting monolithic SiC aerogel exhibited a typical mesoporous structure and exhibited the highest surface area and pore volume compared to all other monolithic aerogels.[100]

The sol–gel method stands as a flexible and effective means for producing SiC nanomaterials with precise control over their size, morphology, and composition.[101,102] The careful selection of precursors, solvents, and process parameters enables this level of control. Moreover, the use of appropriate characterization techniques enables researchers to assess and optimize the quality of the synthesized SiC nanomaterials. The ongoing development and utilization of SiC nanomaterials synthesized *via* the sol–gel method hold great promise for a wide range of applications in various scientific and engineering fields. However, challenges related to reactivity, complexity, lack of mechanistic understanding, and necessary post-processing steps must be carefully considered. These factors should be critically evaluated when selecting preparation techniques suitable for distinct applications or specific material requirements.

5.1.3 Template method. The template method offers a structured approach to crafting SiC nanomaterials, relying on

the use of templates that can be categorized as either hard or soft. Hard templates encompass nanoporous materials and porous structures, serving as sacrificial guides for precise SiC growth. In contrast, soft templates, such as surfactant-assisted self-assembly and co-assembly, harness molecular self-assembly to form organized structures that subsequently function as templates for SiC nanomaterial synthesis.

For SiC nanomaterial preparation using the hard template method, the initial step involves selecting a suitable template material. Subsequently, precursor materials, typically comprising a silicon source and a carbon source, are introduced into the template structure. A high-temperature process is then employed to promote the reaction between the precursor materials, yielding SiC nanomaterials within the template structure. The final step entails the removal of the template material through etching. Commonly used hard template materials include anodized aluminum oxide, zeolite molecular sieves, mesoporous materials and carbon nanotubes.[103–107] An illustrative example of this approach is found in Kim *et al.*'s successful synthesis of SiC microtubes from a wood template with unidirectional pores. The resulting SiC microtubes exhibit a morphology characterized by the presence of villus-like and radial grains on their outer surface, and display fine grains on their inner surface (shown in Fig. 6a).[108] Similarly, Zhao *et al.* have achieved the successfully synthesis of highly ordered mesoporous SiC ceramics by utilizing commercial polycarbosilane as the precursor and mesoporous silica as hard templates.[109] Additionally, Xu *et al.* employed the radio frequency magnetron sputtering technique to fabricate peri-
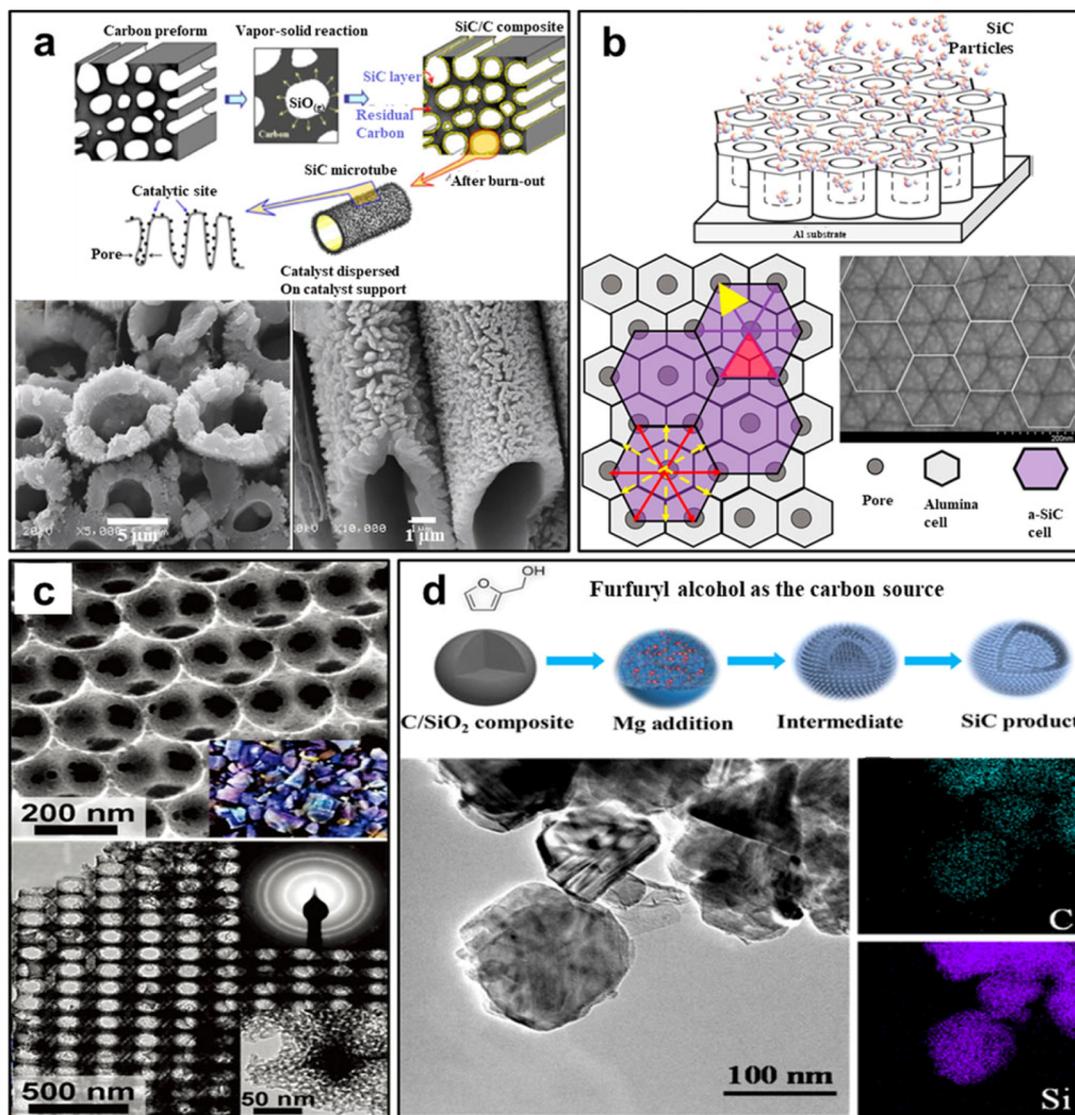
Fig. 6 (a) The synthesized SiC microtubes sample from a wood template. Reprinted with permission from ref. 108. Copyright 2006 by Elsevier and Copyright Clearance Center; (b) periodic SiC nanostructures on AAO templates. Reprinted with permission from ref. 110. Copyright 2020 by Elsevier and Copyright Clearance Center; (c) ordered hierarchical macro-mesoporous SiC nanocomposite. Reprinted with permission from ref. 111. Copyright 2010 by American Chemical Society; (d) mesoporous SiC nanoparticles with high surface area. Reprinted with permission from ref. 112. Copyright 2018 by American Chemical Society.

odic SiC nanostructures on anodic aluminum oxide (AAO) templates, with the presence of defects, especially point defects, on the AAO templates significantly affecting the periodic structure of SiC (shown in Fig. 6b).[110]

Transitioning to the soft template approach for the synthesis of SiC nanomaterials involves a series of steps, including template synthesis, precursor incorporation, self-assembly, template removal, transformation, stabilization, and characterization. This comprehensive process enables the controlled production of SiC nanomaterials with customized sizes, shapes, and properties.[113–116] Stucky *et al.*, for instance, present SiC material featuring an ordered hierarchical macro-mesoporous (OHM) structure, achieved by employing dual templates of Pluronic F127 block copolymer and polystyrene spheres.[111] As depicted in Fig. 6c, the OHM-SiC displays ordered micropores with pore diameters of approximately 230 nm, and TEM images reveal mesopores within the OHM-SiC framework. A selected area electron diffraction (SAED) pattern (Fig. 6c inset) shows distinct concentric rings corresponding to the (111), (220), and (311) diffraction peaks of 3C-SiC. Favier *et al.* have synthesized mesoporous SiC with tunable pore sizes using the triblock copolymers P123 and F127 as soft template,[117] observing that pore sizes decreased as the C/Si ratio in the precursor increased. In a similar vein, Yao *et al.* crafted mesoporous SiC nanostructures through magnesiothermic reduction of C/SiO$_2$ nanocomposites fabricated using P123 as a soft template (shown in Fig. 6d).[112]

The template method presents a versatile and effective avenue for generating SiC nanomaterials, enabling precise control over their size, morphology, and functionalities, particularly ordered porous structures. The adaptability allows for the tailoring of SiC nanomaterials properties, opening doors to diverse applications across various fields. Ongoing research and development in this domain hold significant potential for the advancing SiC nanomaterials and their integration into practical devices and systems. However, challenges associated with template selection, deletion, composition fluidity, and template synthesis act as impediments to the template method. Thoughtful consideration of these elements during material preparation method selection is crucial for specific application or material specifications.

5.2 Vapor-phase synthesis method

Vapor-phase synthesis stands as a controlled process for depositing thin films or coatings onto a substrate, achieved through the reaction of volatile precursor gases. It has emerged as the predominant route for crafting SiC nanomaterials, particularly one dimensional (1D) nanostructure like nanowires, nanorods, and nanoneedles. Within the realm of SiC material synthesis, vapor-phase synthesis offers numerous advantages, notably the capacity to generate high-purity, top-quality films with excellent uniformity and precise manipulation of material properties. Several key parameters, including temperature, heating rate, bias pressure, carrier gas and substrate type, govern the growth of SiC nanostructures. As previous research has documented, techniques such as pyrolysis of polymeric precursors, carbothermal reduction,

chemical vapor deposition (CVD), and thermal evaporation[118] have all been harnessed for SiC nanomaterials fabrication. Essentially, the growth of nanostructures using the aforementioned techniques is always governed by two primary processes: the vapor–liquid–solid (VLS) mechanism and the vapor–solid (VS) mechanism.

5.2.1 Vapor–liquid–solid method. The VLS process, initially developed for Si whisker growth,[119] relies on metal nanoparticles as catalysts to govern the development of 1D nanostructures.[120–122] This process unfolds with the creation of catalyst droplets at high temperatures, followed by the adsorption and dissolution of gaseous species, culminating in the precipitation of solid nanowires. Evidence of VLS growth manifests through the presence of metal droplets at the tips of the resultant nanowires. These metal droplets serve as containment zones, dictating nanowire diameters and final shapes. By adjusting the catalyst droplet sizes, researchers can finely regulate the dimensions and configurations of the resulting nanowires.[123,124]

Chen and co-workers[125] have presented a schematic diagram of SiC 1D nanostructures' synthesized based on VLS mechanism (see Fig. 7a). They claim that the shape of the resulting SiC nanowire is determined by the size of the catalytic droplet. Additionally, they state that factors such as the quantity and arrangement of catalysts, temperature, cooling rate, carrier gas, bias pressure, and substrate surface properties influence the size of the catalytic droplet. Wang and co-workers[126] manipulated catalyst droplet sizes by adjusting applied pressure, enabling precise control over the dimensions and morphology of VLS-grown SiC nanowires (see Fig. 7b).
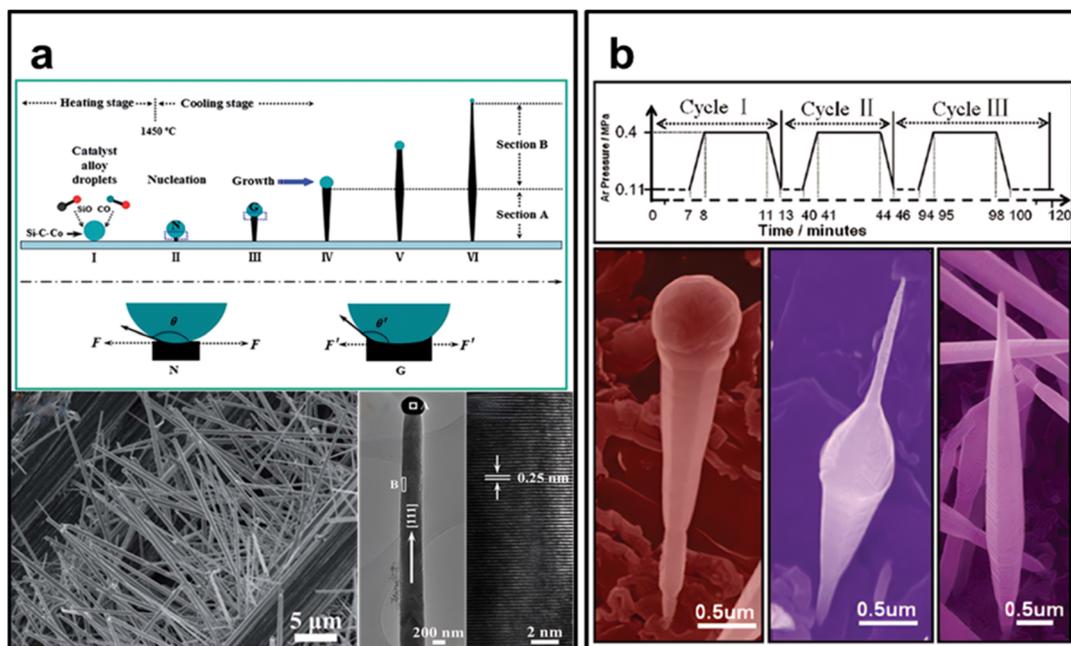

Fig. 7 (a) Controlled growth of quasialigned SiC nanoarrays with clear and sharp tips. Reprinted with permission from ref. 125. Copyright 2014 by Royal Society of Chemistry; (b) manipulate and control the morphology of SiC nanowires by varying the pressure of the source species. Reprinted with permission from ref. 126. Copyright 2008 by Royal Society of Chemistry.

Additionally, Liu and colleagues developed an *in situ* VLS preparation method for SiC whiskers (SiCw) utilizing Fe-oxides as catalysts on carbon fibers. The resulting SiCw are β-SiC, growing along the (111) crystal plane, with Fe_2O_3 catalysts forming spherical droplets at the apex. These SiCw measure 500–1000 nm in width and exceed 15 μm in length. Okumura *et al.* reported the successful incorporation of Pt into Si-based flux in the VLS process for the growing 4H-SiC epitaxial films. This addition effectively suppresses step bunching and promotes the step-flow growth mode. Furthermore, the resulting SiC film surface exhibits remarkable flatness, featuring well-defined step-and-terrace structures with narrow terrace widths and straight step lines.

The VLS method boasts numerous advantages compared to other SiC synthesis techniques. These benefits encompass simplicity, scalability, and cost-effectiveness. It allows for SiC production in various forms, including powders, fibers, and single crystals. Another noteworthy advantage is the ability to exert control over material properties such as crystal structure, size, and purity. However, the VLS method also presents limitations and challenges, including the necessity for high temperatures, extended processing times, and the potential for impurity incorporation. Controlling crystal size and morphology can prove challenging, impacting the overall material quality.

5.2.2 Vapor–solid method. The VS method involves the introduction of a silicon precursor and a carbon source into a high-temperature furnace. The ensuing reaction between the precursor and the carbon source yields gaseous SiC, which then condenses on a cooler surface, giving rise to SiC crystals. The VS method can be further classified into subcategories such as chemical vapor deposition (CVD), physical vapor deposition (PVD), and other related techniques. This method offers several advantages, including high purity, control over stoichiometry, and the ability to obtain SiC films on various substrates.

Wang *et al.* synthesized SiC tubes through a straightforward VS reaction growth pathway employing vaporized $MeSiHCl_2$ to react with calcium deposited on silicon (shown in Fig. 8a). This reaction follows a solvent-free Yajima-type process at the vapor–solid interface.[127] Ren *et al.* successfully synthesized SiC nanowhiskers on carbonized coconut fiber surfaces using a VS mechanism within the temperature range of 1300–1500 °C, employing photovoltaic silicon waste and quartz sand (as a hybrid silicon source), and coconut fiber as a carbon source.[128] Li *et al.* reported large-scale fabrication of single-crystal SiC nanowire sponges using agricultural residue loofah (see Fig. 8b). They systematically investigated the underlying vapor–solid mechanism through thermodynamic calculations on the formation and interactions of SiO, CO, and SiC.[129] Chen *et al.* reported a large number of single crystalline SiC nanowires with lengths extending to several tens of micrometers and diameters of 20–60 nm, employing a simple catalyst-free method that utilized silicon powders and expandable graphite as raw materials.[130]
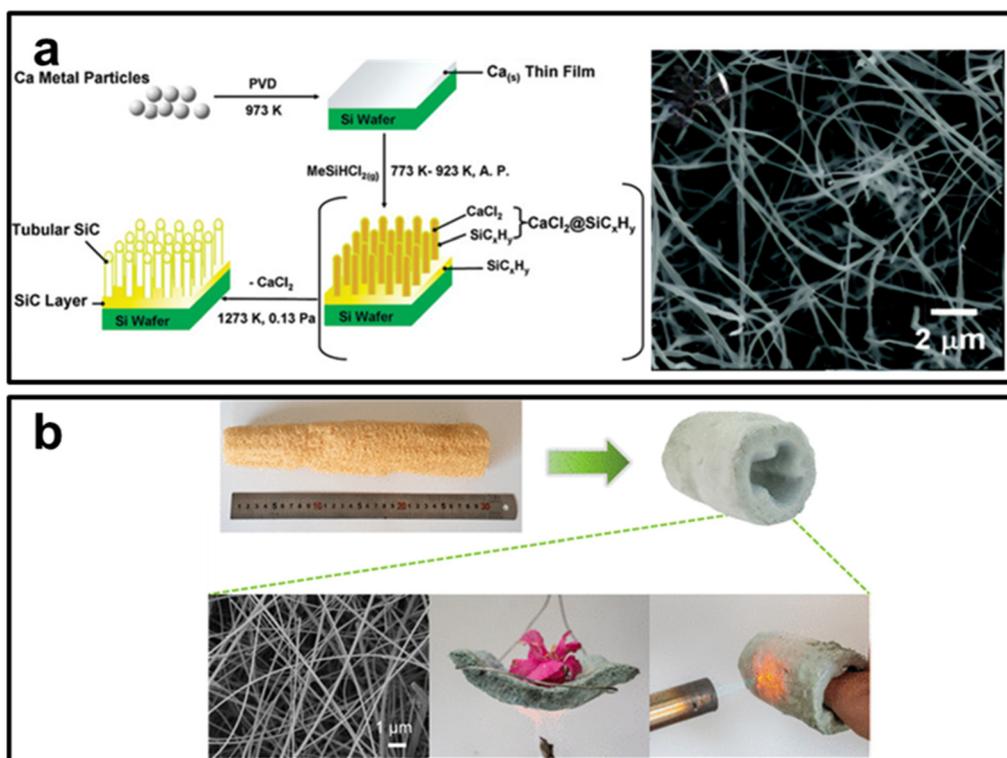

Fig. 8 (a) Large-scale fabrication of single–crystal SiC nanowire sponges using agricultural residue loofah.Reprinted with permission from ref. 127. Copyright 2007 by American Chemical Society; (b) long SiC nanowires grow in the specified direction. Reprinted with permission from ref. 129. Copyright 2023 by American Chemical Society.

The VS method has many benefits compared to other SiC synthesis techniques. These advantages include simplicity, scalability, and cost-effectiveness. It enables the production of SiC in different forms like powders, fibers, and single crystals. Another significant advantage is the ability to control material properties such as crystal structure, size, and purity. However, the VS method also has limitations and challenges. These include the requirement for high temperatures, long processing times, and the possibility of impurity incorporation. It can be difficult to control crystal size and morphology, which can affect the overall quality of the material. Liquid-phase synthesis method.

The above methods of fabricating SiC nanomaterials, including solid-phase and vapor-phase techniques that necessitate temperatures exceeding 800 °C, come with the drawbacks of costly production processes and limited scalability. Additionally, these techniques are often unsuitable for the majority of organic materials. Consequently, the quest for low-temperature techniques to produce SiC nanocrystals emerges as a viable solution to reduce the expenses associated with industrial production. Liquid-phase synthesis of SiC nanomaterials predominantly encompasses solvothermal[131,132] and electrochemical etching[133,134] methods.

5.2.3 Solvothermal method. The solvothermal synthesis technique involves the utilization of solvents such as inorganic, organic, or aqueous medium, in a sealed system which is maintained at a predetermined temperature. For instance, Zou et al. reported the synthesis of SiC nanoflakes, exhibiting diameters ranging from 200 to 500 nm and a thickness of approximately 15 nm, using a one-step solvothermal method. This method involved the reaction of $SiCl_4$ and CaC at a temperature of 180 °C.[135] Chen et al. reported the synthesis of SiC hollow nanospheres and nanowires at 600 and 700 °C, respectively, utilizing $SiCl_4$ and C_6Cl_6 as source materials and metallic sodium as the reductant. Their studies revealed that temperature and reagents played pivotal roles in determining the morphologies of the resulting products.[136] Lu et al. reported an efficient method for the synthesis of β-SiC nanorods via a one-step reaction under pressure at a temperature of 400 °C.[137] This method employed $SiCl_4$ and CCl_4 as reactants, alongside a metallic sodium as a coreductant, within an autoclave. The resulting product exhibited nanorod features with varying diameters ranging from 10 to 40 nm, and lengths extending up to several micrometers. Additionally, Zhang reported the quasi-monodisperse β-SiC nanospheres synthesized in a hexane and water mixed solvent at 180 °C using a composite surfactants-assisted mix-solvothermal route. The size of β-SiC nanospheres could be effectively adjusted by modifying the hexane/water ratio, as depicted in Fig. 9a.[138]

The solvothermal technique proves facile in fabricating high-purity, uniform carbon–silicon composites with precise particle size control. Nonetheless, it confronts complexities, reproducibility, expense, and environmental ramifications which need careful consideration during selection.

5.2.4 Electrochemical etching method. The electrochemical etching process involves the controlled dissolution of SiC substrates in an electrolyte solution under the influence of an electric field.[139] This technique offers several advantages over other fabrication methods, such as high precision, room temperatures, atmospheric pressure, and simplicity. Diverse SiC nanostructures with tailored dimensions and morphologies can be achieved by adjusting etching parameters such as applied voltage, current density, and etching time.[140] For instance, Van Dorp et al. discovered that anodic dissolution and passivation occurred for p-type electrodes in the dark and for n-type electrodes under illumination when studying electrochemical etching of single-crystal SiC rotating disk electrodes in a fluoride solution at pH 3.[141] Xu et al. synthesized an integrated self-supporting 4H-SiC nanohole array using a 4H-SiC anode, graphite cathode, and a C_2H_5OH, HF, and H_2O_2 electrolyte solution. The SiC sheet anode underwent electrochemical etching in pulsed-voltage mode, with a fixed voltage of 19 V and a pulsed cycle time of 0.8 s, followed by a pause time of 0.4 s.[142] Zhao et al. reported a method for large-scale fabrication of free-standing and transparent SiC nanohole array with tailored structures via anodic oxidation of SiC wafers at room temperature and atmospheric pressure conditions. They discovery that the cycle period of the pulsed voltage significantly influenced the formation of highly uniform nanohole arrays, as depicted in Fig. 9b.[143]

In summary, electrochemical etching offers an efficient strategy for fabricating SiC nanomaterials with precise physical dimensions and morphologies. The technique presents advantages such as simplicity of execution, affordability, and eco-friendliness. However, it is essential to acknowledge issues related to replicability, limited applicability, and scalability. To leverage the potential of this method in SiC nanomaterial creation, careful consideration of its unique pros and cons is necessary, aligning them with specified needs and material requisites.

6 Supercapacitor applications

Supercapacitors, also known as electrochemical capacitors or ultracapacitors, represent a class of energy storage devices that bridge the gap between traditional capacitors and batteries. They rely on two primary principles for energy storage:[144,145] (a) *Double-layer capacitance*. This principle involves the storage of charge at the interface between the electrode and the electrolyte. Energy storage primarily depends on the physical separation of charges within the electric double layer formed at the electrode–electrolyte interface.[145,146] (b) *Faradaic processes*. Faradaic processes occurs due to reversible reactions at the electrode–electrolyte interface, resulting in charge storage through redox reactions.[26] This involves the use of electrochemically active materials on the electrode surface, surpassing the energy storage limitations of double-layer capacitance.[147]

Supercapacitors offer several significant advantages when compared to other energy storage technologies. (a) *High power density*: supercapacitors can deliver and absorb a significant amount of power rapidly due to their low internal resistance.
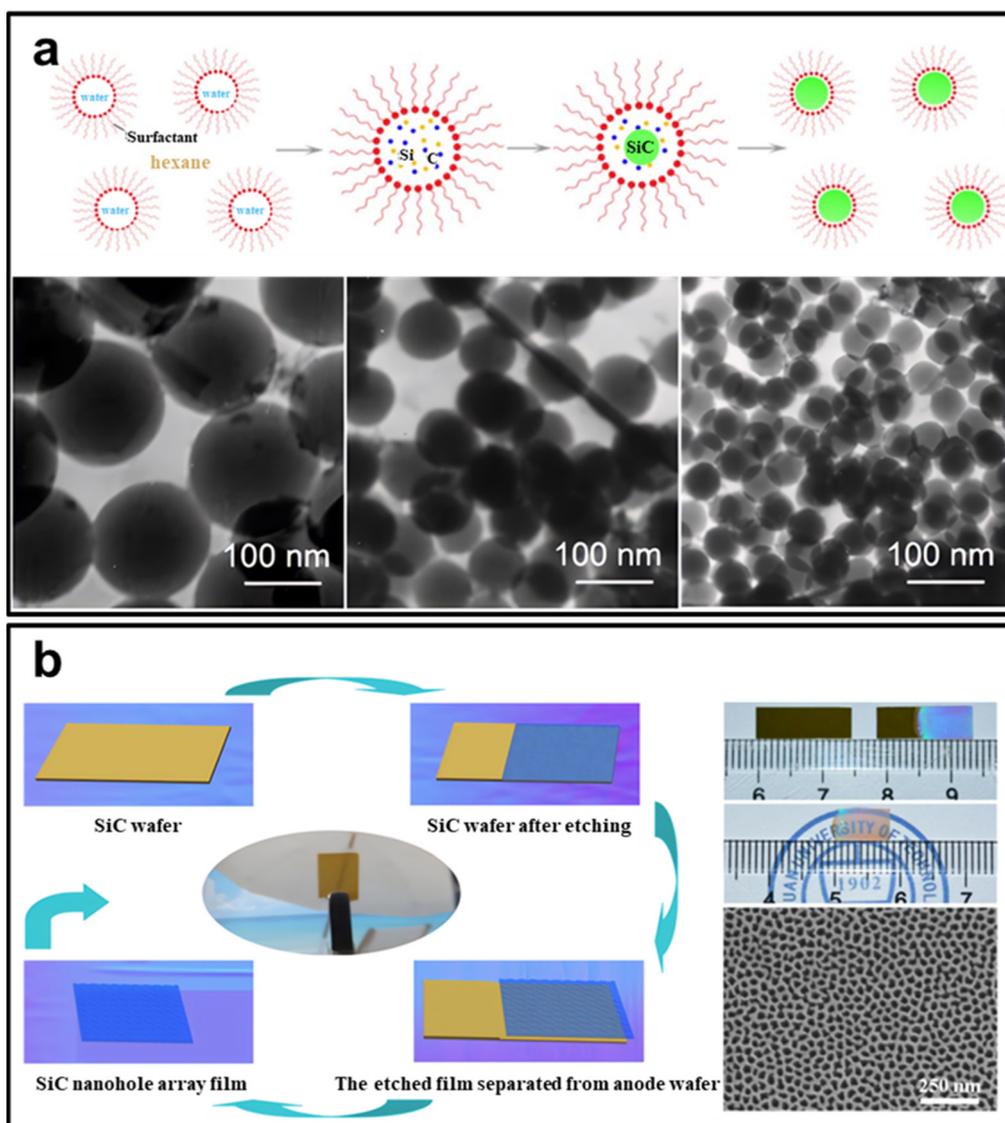
Fig. 9 (a) The morphology and size of SiC nanospheres synthesized with varying hexane/water volume ratio. Reprinted with permission from ref. 138. Copyright 2017 by Elsevier and Copyright Clearance Center; (b) large-scale fabrication of free-standing and transparent SiC nanohole array with tailored structures. Reprinted with permission from ref. 143. Copyright 2018 by Elsevier and Copyright Clearance Center.

This makes them suitable for applications requiring rapid energy release, such as electric vehicles and regenerative braking systems.[148,149] (b) *Rapid charging and discharging*: supercapacitors exhibit exceptional charge and discharge rates, enabling quick energy storage and release. Unlike batteries with longer charging times, supercapacitors can be charged within seconds or minutes, reducing downtime and enhancing efficiency.[150,151] (c) *Long cycle life*: supercapacitors have a substantially longer cycle life compared to conventional batteries, enduring thousands or even millions of charge–discharge cycles without significant degradation. This reduces maintenance costs and extends the operation lifetime of energy storage systems.[152,153] (d) *Wide operating temperature range*: supercapacitors maintain excellent performance across a broad range of operating temperatures, making them suit-

able for applications in extreme environmental conditions, such as aerospace and automotive industries.[154,155]

Supercapacitors employing SiC electrodes have garnered considerable attention due to their unique properties and potential for enhanced performance. To optimize their performance, future research should focus on material modifications, electrode design optimization, electrolyte selection, and scalable manufacturing processes.[156]

6.1 Supercapacitors with SiC nanomaterials electrodes

The morphology and porous structure of SiC play a crucial role in enhancing supercapacitor performance. The morphology of SiC materials governs their surface area and porosity, both of which are key factors influencing supercapacitor performance. Nanosized SiC particles offer a high surface area, resulting in

an increased capacitance. As the size of SiC particles decreases, more sites for charge storage become available due to the higher surface area. However, smaller particles may also lead to increased internal resistance in the supercapacitor, attributed to the higher tortuosity of the charge-transport pathways. Therefore, a balance must be struck between particle size and the desired performance characteristics of the supercapacitor.

The presence of porosity in SiC adds another dimension to its potential as an effective supercapacitor material. Porous SiC structures not only provide a high surface area but also allow for efficient ion diffusion and mass transport. The pores serve as charge-storage sites, increasing capacitance, while also providing channels for the facile transport of electrolyte ions. The pore size and distribution have a crucial impact on the supercapacitor performance. For example, microporous SiC materials feature short diffusion paths, which result in excellent charge–discharge behavior at high rates. Conversely, macroporous SiC materials offer high capacitance values due to their large pore volume and accessible surface area.

Furthermore, controlling the porosity and pore size of SiC allows for tailored electrochemical properties. For example, mesoporous SiC materials feature interconnected pores that not only enhance ion diffusion but also allow for an increase in the accessible surface area, leading to a commensurate increase in capacitance. The hierarchical structure, combining both micropores and macropores, can offer superior charge-storage capabilities while maintaining good mass transport properties.

In summary, nanomorphology and porous structure provide a large surface area, increasing the active electrode–electrolyte interface for efficient charge storage and transfer. These structures facilitate electrolyte ion access, promoting rapid diffusion and adsorption onto the electrode surface. Consequently, this leads to improved charge storage capacity

and faster charging and discharging rates of the supercapacitor. Additionally, the interconnected porous network reduces internal resistance, resulting in lower energy losses during charge and discharge cycles, thus enhancing power density and overall efficiency. Understanding and optimizing these properties is crucial for the development of high-performance SiC-based supercapacitors. Many researchers have actively explored various porous SiC nanomaterials to create tailored porous structures that maximize the performance of supercapacitors. Table 1 summarizes the electrochemical performance of supercapacitors employing SiC nanomaterials as electrode.

The successful preparation and application of SiC with different morphologies in supercapacitors have been achieved. Here, we provide a brief review of several representative literature on this topic. For example, Kim *et al.* reported hierarchically micro and mesoporous silicon carbide frameworks (MMPSiC) with a three-dimensional structure synthesized through a template method and carbonization reaction utilizing aerosol-spray drying (see Fig. 10a).[161] MMPSiC exhibits facilitating faster ion transport behavior and larger utilization of the surface area of electric double-layer capacitors. The specific capacitance is 253.7 F g^{-1} in 1 M Na_2SO_4 aqueous electrolyte at 5 mV s^{-1}. Additionally, it registers a specific capacitance of 40.3 F g^{-1} in 3-ethyl-3-methylimidazolium bis(trifluorosulfonyl)imide ionic-liquid electrolyte at 5 mV s^{-1}, providing an energy density of 68.56 W h kg^{-1}, with ~98.4% of specific capacitance remaining over 20 000 cycles. Sanger *et al.* successfully developed a symmetric supercapacitor with a SiC nanocauliflowers as electrode material using reactive DC sputtering technique (Fig. 10b).[164] The supercapacitor exhibits remarkable performance, with a high specific capacitance of 188 F g^{-1} at 5 mV s^{-1}, as well as excellent cycling stability with 97.05% capacitance retention after 30 000 cycles. Additionally, it boasts high energy density (31.43 W h kg^{-1}) and power

Table 1 Performances of SiC nanomaterials-based supercapacitors

| Electrode materials	Current collectors	Electrolyte	Specific capacitance	Ref.
SiC nanowires	Carbon fabric	KCl (2 M)	23 mF cm^{-2} (at 50 mV s^{-1}, three-electrode)	157
SiC nanowires	Silicon substrate	KCl (3.5 M)	240 mF cm^{-2} (at 100 mV s^{-1}, three-electrode)	158
Nitrogen Doped SiC Nanoarray	Carbon fabric	KCl (3 M)	4.8 mF cm^{-2} (at 10 mV s^{-1}, three-electrode)	159
3C-SiC nanowire film	Graphite paper	H_2SO_4 (0.1 M)	37 mF cm^{-2} (at 0.3 A cm^{-2}, two-electrode)	160
SiC nanowire	Silicon wafer	Yttria-stabilized zircon	92 µF cm^{-2} (at 100 mV s^{-1}, two-electrode), 350 °C	64
Micro- and mesoporous SiC sphere	Aluminum foil	Na_2SO_4 (1 M)	253.7 F g^{-1} (at 5 mV s^{-1}, three-electrode)	161
SiC porous nanofiber membranes	Nickel foil	KOH (1 M)	189 F g^{-1} (at, 0.2 A g^{-1}, three-electrode)	162
Porous SiC flakes	Stainless steel foil	KCl (1 M)	49.2 F g^{-1} (at 5 mV s^{-1}, two-electrode)	163
SiC nanocauliflowers	Ag coated porous alumina	Na_2SO_4 (1 M)	188 F g^{-1} (at 5 mV s^{-1}, two-electrode)	164
4H-SiC nanochannel array	Self	KCl (2 M)	14.8 mF cm^{-2} (at 10 mV s^{-1}, two-electrode)	165
SiC nanowire arrays	Self	PVA/KCl gel	22.3 mF cm^{-2} (at 10 mV s^{-1}, two-electrode)	53
3C-SiC/graphene	Silicon substrate	H_2SO_4 (0.5 M)	8.533 mF cm^{-2} (at 20 µA cm^{-2}, three-electrode)	166
SiC nanowires	Carbon fabric	KCl (2 M)	46.7 mF cm^{-2} (at 0.1 V s^{-1}, three-electrode)	167
Porous SiC/C	Nickel foam	KOH (6 M)	194.8 F g^{-1} (at 0.2 A g^{-1}, two-electrode)	168
SiC nanofibers	Carbon fabric	KCl (2 M)	4.36 mF cm^{-2}, (at 50 mV s^{-1}, two-electrode)	169
SiC nanowires	Carbon fabric	KCl (2 M)	23.6 mF cm^{-2} (at 0.2 mA cm^{-2}, two-electrode)	50
3C/2H/6H heterojunction SiC nanowires	Nickel foam	KCl (2 M)	227.8 F g^{-1} (at 10 mV s^{-1}, three-electrode)	51
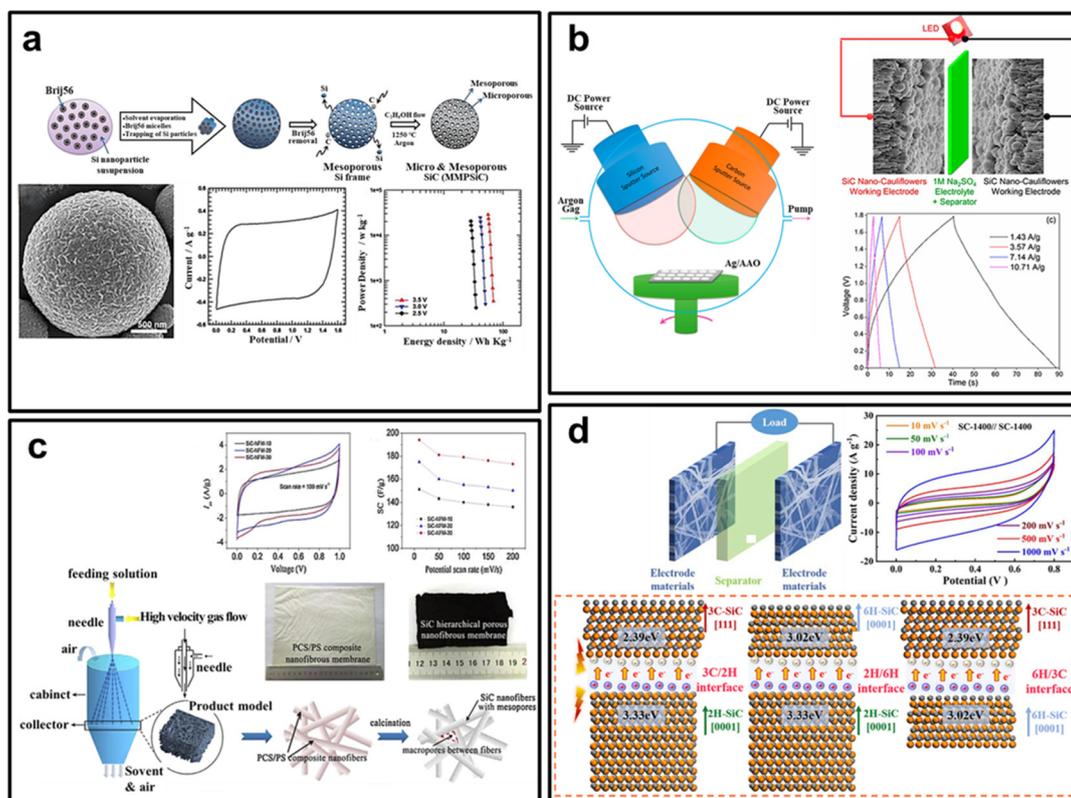
Fig. 10 Supercapacitors with SiC nanomaterials electrodes. (a) micro- and mesoporous SiC sphere. Reprinted with permission from ref. 161. Copyright 2015 by Royal Society of Chemistry; (b) SiC nanocauliflowers. Reprinted with permission from ref. 164. Copyright 2016 by American Chemical Society; (c) SiC porous nanofiber membrane. Reprinted with permission from ref. 162. Copyright 2016 by Elsevier and Copyright Clearance Center; (d) 3C/2H/6H heterojunction SiC nanowires. Reprinted with permission from ref. 51. Copyright 2023 by Royal Society of Chemistry.

density ($\sim$18.8 kW kg^{-1} at 17.76 W h kg^{-1}) within a voltage range of 1.8 V. Zhao *et al.* reported SiC nanofiber membranes (SiC-NFMs) with a porous architecture prepared *via* a solution blowing process and subsequent calcination (Fig. 10c).[162] The supercapacitor based on SiC-NFMs as electrode materials demonstrated excellent specific capacitance ($\sim$189 F g^{-1}) and outstanding cycling stability (91.7% retention after 3000 cycles). The authors believe that the porous architecture of SiC-NFMs, which was composed of mesopores in each single nanofiber and macropores between nanofibers, led to the excellent electrochemical performance.[162] Kang *et al.* reported a novel method to enhance the performance of SiC nanowires (SiC NWs) for electrochemical energy storage (Fig. 10d).[51] They created SiC NWs with a heterostructured combination of 3C-, 2H-, and 6H-SiC and a conductive network with a high specific surface area using a simple thermal evaporation method. By leveraging the synergistic effects of these multiple structures, they significantly improved the electrochemical properties of the SiC NWs, achieving a specific capacitance of 227.8 F g^{-1} at 10 mV s^{-1}. Furthermore, they assembled a symmetrical supercapacitor using these optimized SiC NWs, which retained as high as 90.12% of its capacitance after 10 000 cycles.

Nanotechnology not only enhances the specific capacitance of SiC-based supercapacitors, but also broadens their applications in various aspects. Researchers have explored novel

uses for SiC-based supercapacitors, harnessing their unique properties for specialized functions. One notable application is the development of high-temperature supercapacitors (supercapacitors) using SiC nanowires as electrode materials. Yang *et al.* reported on this advancement, where etched SiC nanowires were employed to fabricate electrodes. These electrodes exhibited a specific capacitance of 23.6 mF cm^{-2} at 0.2 mA cm^{-2}. More impressively, ionic-liquid-based supercapacitors constructed with these SiC nanowires could withstand operating temperatures of up to 150 °C, maintaining a capacitance retention of 80% over 10 000 cycles. Even when subjected to progressive temperature variations ranging from 0 to 150 °C, the capacitance retention remained above 76% for 12 000 cycles. This innovation opens doors for SiC-based supercapacitors in demanding high-temperature environments (Fig. 11a).[50]

Another breakthrough comes from Chang *et al.*, who designed a symmetric supercapacitor using yttria-stabilized zirconia (YSZ) as the electrolyte and SiC nanowires as the electrode. These stacked symmetric SiC nanowires/YSZ/SiC nanowires supercapacitors demonstrated exceptional thermal stability and high areal capacitance, particularly at temperatures exceeding 300 °C. Remarkably, they continued to function efficiently even at temperatures reaching up to 450 °C, delivering an impressive areal capacitance of 92 μF cm^{-2} at 100 mV s^{-1}. This achievement expands the use of SiC-based
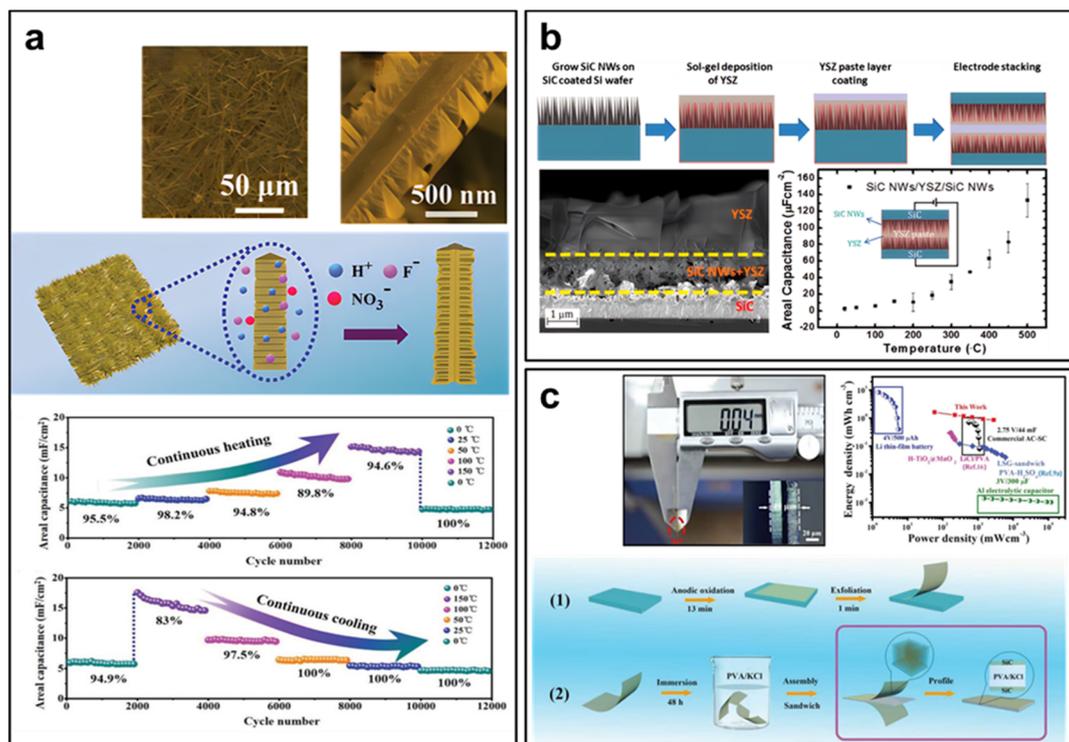
Fig. 11 (a) Robust high-temperature supercapacitors based on SiC nanowires. Reprinted with permission from ref. 50. Copyright 2021 by John Wiley and Sons and Copyright Clearance Center; (b) all solid-state microsupercapacitors based on SiC nanowire electrode and YSZ electrolyte. Reprinted with permission from ref. 64. Copyright 2015 by American Chemical Society; (c) all-solid-state on-chip supercapacitors based on free-standing 4H-SiC nanowire arrays. Reprinted with permission from ref. 53. Copyright 2019 by John Wiley and Sons and Copyright Clearance Center.

supercapacitors into extreme-temperature applications, such as aerospace and industrial processes (Fig. 11b).[64]

Li *et al.* presented a novel approach to high-performance all-solid-state SiC supercapacitors. These supercapacitors were based on free-standing SiC nanowire arrays fabricated using an anodic oxidation process. Unlike conventional designs, these supercapacitors featured a solid electrolyte layer sandwiched between two pieces of SiC nanowire arrays film, eliminating the need for a substrate. These supercapacitors achieved impressive specific area energy and power density values of 5.24 μW h cm^{-2} and 11.2 mW cm^{-2}, respectively. Furthermore, their specific volume energy and power density reached 1.31 mW h cm^{-3} and 2.8 W cm^{-3}, respectively. Notably, the on-chip supercapacitors exhibited excellent rate capability and robust stability, with over 94% capacitance retention after 10 000 cycles at 100 mV s^{-1}. This innovation holds great promise for applications requiring miniaturization and all-solid-state energy storage solutions (Fig. 11c).[53]

These advancements in SiC-based supercapacitor technology showcase their versatility and potential for use in extreme conditions and emerging technologies, expanding their scope beyond traditional energy storage applications.

In this summary, supercapacitors using SiC nanomaterial electrodes offer several advantages. Firstly, SiC nanomaterials showcase exceptional mechanical and chemical stability, ensuring durability and a prolonged lifespan for the super-

capacitor in dynamic environments. This durability ensures a lengthy lifetime for the supercapacitor, making it a dependable energy storage device. Secondly, SiC nanomaterials boast a high surface area, significantly enhancing the charge-storage capacity of the supercapacitor. This extensive surface area provides numerous sites for charge accumulation, resulting in superior capacitance. Thirdly, SiC nanomaterials exhibit excellent charge–discharge capabilities, facilitating swift charging and discharging operations. This is attributed to the particle size of SiC, minimizing the diffusion paths for charges, thereby reducing charging and discharging time. Nevertheless, despite these benefits, SiC nanomaterials also present certain drawbacks. Firstly, the synthesis of SiC nanomaterials can be intricate and costly, potentially limiting its ubiquitous application in supercapacitors. Secondly, SiC nanomaterials exhibit relatively low electrical conductivity, increasing the supercapacitor's internal resistance, potentially undermining its overall performance. Thirdly, although SiC nanomaterials possess a high specific surface area, they exhibit relatively low specific capacitance compared to other materials, resulting in lower energy storage capacity. Addressing these limitations is crucial for the successful integration of SiC nanomaterials into practical supercapacitor applications. Further research and development efforts are necessary to overcome these challenges and fully exploit the potential of SiC nanomaterials in energy storage technologies.

Table 2 Performances of SiC-based composites supercapacitors

Electrode materials	Current collectors	Electrolyte	Specific capacitance	Ref.
C–Ni–SiC composite	Unspecified	KOH (1 M)	1780 F g^{-1} (at 8.7 A g^{-1}, three-electrode)	170
Microsphere SiC/nanoneedle MnO$_2$	Nickel foam	Na$_2$SO$_4$ (1 M)	273.2 F g^{-1} (at 10 mV s^{-1}, three-electrode)	171
SiC/B-MnO$_x$	Nickel foam	Na$_2$SO$_4$ (1 M)	251.3 F g^{-1} (at 10 mV s^{-1}, three-electrode)	172
SiC nanowires@Ni(OH)$_2$	Carbon fabric	KOH/PVA gel	4.7 mF cm^{-2} (at 20 mV s^{-1}, two electrode)	160
Modified SiC@SiO$_2$ nanocables/MnO$_2$	Titanium sheet	Na$_2$SO$_4$ (1 M)	276.3 F g^{-1} (at 0.2 A g^{-1}, three-electrode)	173
CoNi$_2$S$_4$ nanosheets-decorated SiC nanowires	Carbon cloth	KOH (6 M)	231.1 mA h g^{-1} (at 2 A g^{-1}, two electrode)	174
NiCo$_2$O$_4$/NiO Nanosheets on SiC Nanowires	Carbon cloth	KOH (6 M)	1499 F g^{-1} (at 10 mA cm^{-2}, three-electrode)	55
Mesoporous C/SiC	Unspecified	KOH (6 M)	220 F g^{-1} (at 1 A g^{-1}, two-electrode)	47
NiSi/SiC core–shell nanowires	Nickel foil	KOH (1 M)	75 mF cm^{-2} (at 100 mV s^{-1}, three-electrode)	175
Micro- and mesoporous SiC/Fe$_3$O$_4$	Nickel-plated polyester fabric	PVA-KOH-p-nitroaniline gel	423.2 F g^{-1} (at 5 mV s^{-1}, two electrode)	176
SiC nanowire @Fe$_2$O$_3$ nanoneedle arrays	Carbon cloth	KOH (2 M)	721 F g^{-1} (at 2 A g^{-1}, three-electrode)	177
SiC nanowire @NiCo$_2$O$_4$/Ni(OH)$_2$ hybrid nanosheet arrays	Carbon cloth	KOH (2 M)	2580 F g^{-1} (at 2 A g^{-1}, three-electrode)	178
SiC coated CuS nanowires	Copper substrates	NaOH (1 M)	3370 F g^{-1} (at 10 mV s^{-1}, three-electrode)	179
Co(OH)$_2$ nanoparticles/Ni$_3$S$_2$ nanosheets-SiC nanowire	Carbon cloth	KOH (6 M)	2318 F g^{-1} (at 6 mA cm^{-2}, three-electrode)	52
SiC@C nanowire arrays	Carbon fabric	KCl (2 M)	78.98 mF cm^{-2} (at 0.2 mA cm^{-2}, three-electrode)	57
NiCo$_2$O$_4$ nanosheets sheathed SiC@CNTs	Carbon cloth	PVA/KOH gel	180 F g^{-1} (at 20 A g^{-1}, two electrode)	180
B-doped SiC/Si	Silicon wafer	H$_2$SO$_4$ (1 M)	232 F g^{-1} (at 2.2 A g^{-1}, three-electrode)	181
NiSi/SiC core–shell nanowires	Nickel foil	KOH (1 M)	234.13 mF cm^{-2} (at 100 mV s^{-1}, three-electrode)	182
Hierarchical porous C/SiC	Glassy carbon plate	Na$_2$SO$_4$ (1 M)	224 F g^{-1} (at, 0.2 A g^{-1}, two-electrode)	183
Co$_3$O$_4$-decorated SiC nano-tree array	4H-SiC wafer	KOH (5 M)	845 mF cm^{-2} (at 10 mV s^{-1}, three-electrode)	184
SiC@Si pyramids	Silicon wafer	NaOH (1 M)	135.5 F cm^{-2} (at 10 mV s^{-1}, three-electrode)	185
SiC nanowires@NiCo$_2$O$_4$ hollow nanocages	Carbon cloth	KOH (1 M)	1377.6 F g^{-1} (at 1 A g^{-1}, three-electrode)	186
SiC nanowires@NiCo$_2$O$_4$ nanoarrays	Carbon cloth	KOH (1 M)	1640.7 F g^{-1} (at 0.5 A g^{-1}, three-electrode)	187
SiC@PANI core/shell nanowire arrays	Carbon fiber	H$_2$SO$_4$ (1 M)	352 mF g^{-1} (at 1 mA cm^{-2}, three-electrode)	188
SiC-decorated B-doped graphene	Nickel foam	NaOH (3 M)	1384.3 mF cm^{-2} (at 3 mA cm^{-2}, three-electrode)	69
C-coated SiC nanosheets	Not provided	Na$_2$SO$_4$ (1 M)	734 μF cm^{-2} (at 10 mV s^{-1}, three-electrode)	56
SiC@PEDOT nanowires	Carbon fabric	KCl (2 M)	6.35 mF cm^{-2} (at 0.05 mA cm^{-2}, two-electrode)	189
Ti$_3$C$_2$T$_x$/SiC heterostructure	self	PVA-Na$_2$SO$_4$	97.8 mF cm^{-2} (at 1 A cm^{-2}, two-electrode)	190
SiC nanowires/carbon nanotubes	Self	1-Butyl-3-methylimidazolium tetrafluoroborate	8.43 F g^{-1} (at 0.02 A g^{-1}, two-electrode)	190
SiC/pyrrolic-N doped carbon	Nickel foam	H$_2$SO$_4$ (1 M)	369 F g^{-1} (at 0.5 A g^{-1}, three-electrode)	191
SiC/C foams	Self	NaCl (3 M)	78.07 F g^{-1} (at 10 mV s^{-1}, three-electrode)	192

6.2 Supercapacitors with SiC-based composite electrodes

While SiC exhibits remarkable electrical and chemical properties as a supercapacitor electrode material, its specific capacitance is relatively lower than other electrode materials like metal oxides and hydroxides. This limitation restricts the overall energy storage capacity of SiC-based supercapacitors. To overcome these limitations and make full use of the excellent properties of SiC, the development of SiC-based composite nanomaterials has gained significant attention. By incorporating SiC nanomaterials with other functional materials, such as conductive polymers, metal oxides, or carbon nanomaterials and so on (see Table 2), the resulting composites can address the challenges associated with SiC electrodes, including enhancing specific capacitance, increasing cycling stability, and improving overall electrochemical performance.

The remarkable properties of SiC, characterized by its robust mechanical strength and resistance to chemical and electrochemical degradation, make SiC-based composite supercapacitors exceptionally reliable and suitable for long-term energy storage applications. In a groundbreaking development, Ma *et al.* introduced a novel approach to improve SiC-based supercapacitors.[191] They reported the reparation of SiC/N dual doped bio-renewable carbon material, utilizing bio-renewable bamboo as the sacrificial template and a dopant (Fig. 12a). This innovation involved the dual doping of SiC and pyrrolic-N species, which facilitated faradaic redox reactions during charge/discharge process. As a result, it significantly enhanced the rate capability at higher current densities, while also exhibiting excellent electrochemical stability. The derived SiC/N dual doped carbon electrode material showcased remarkable capacitive behavior, boasting a capacitance of 369 $F\ g^{-1}$ at 0.5 $A\ g^{-1}$ in a 1 M H_2SO_4 electrolyte. Impressively, it retained 100% of its capacitance after 5000 charge–discharge cycles. Furthermore, symmetric supercapacitors assembled with these SiC/N dual doped carbon electrodes exhibited outstanding capacitance of 162 $F\ g^{-1}$ at 0.5 $A\ g^{-1}$, high energy
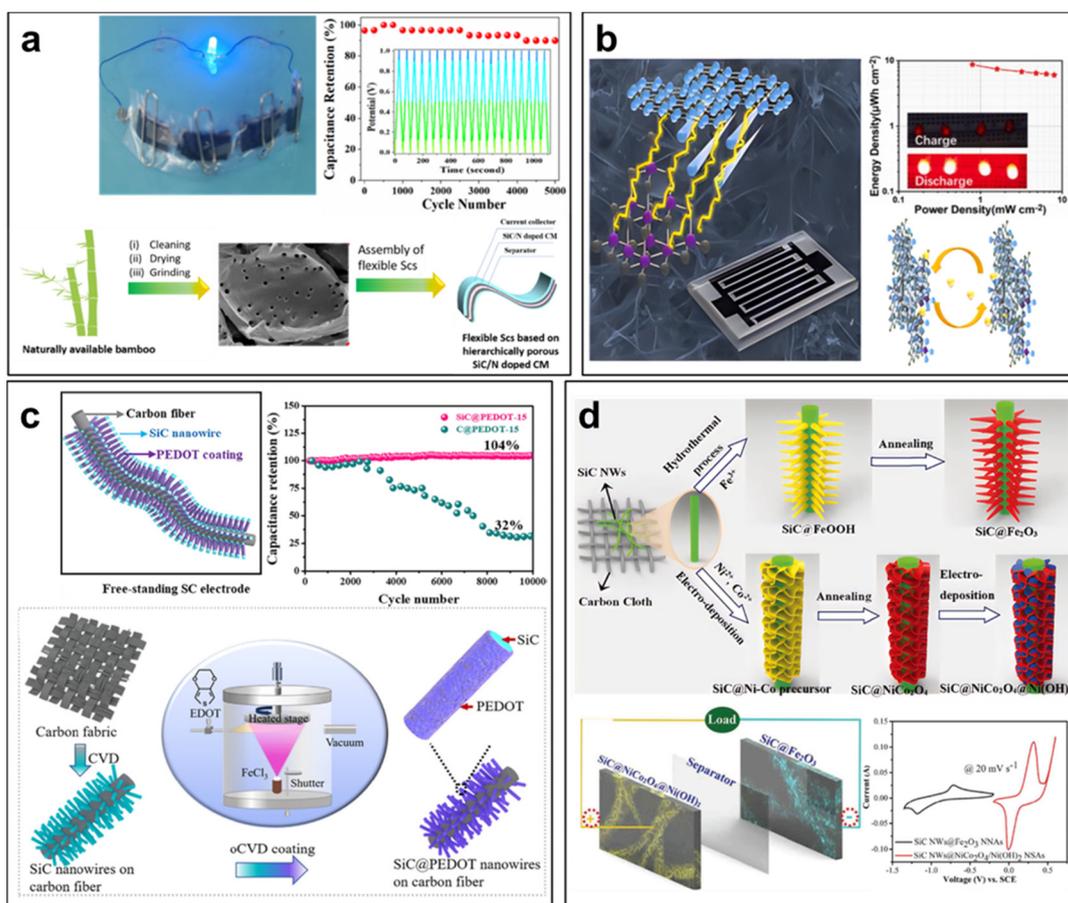

Fig. 12 (a) Bamboo-derived carbon material inherently doped with SiC and nitrogen for flexible supercapacitors. Reprinted with permission from ref. 191. Copyright 2022 by Elsevier and Copyright Clearance Center; (b) MXene/SiC heterostructure for micro-supercapacitor. Reprinted with permission from ref. 189. Copyright 2022 by Elsevier and Copyright Clearance Center; (c) Supercapacitors based on free-standing SiC@PEDOT Nanowires. Reprinted with permission from ref. 56. Copyright 2022 by Elsevier and Copyright Clearance Center; (d) asymmetric supercapacitor based on Fe_2O_3 nanoneedle arrays and $NiCo_2O_4/Ni(OH)_2$ hybrid nanosheet arrays grown on SiC nanowire networks. Reprinted with permission from ref. 177. Copyright 2018 by John Wiley and Sons and Copyright Clearance Center.

density (~5.41 W h kg^{-1} at 0.5 kW kg^{-1} power density), and excellent cyclic stability.

While MXene micro-supercapacitors hold great potential for energy storage, addressing the challenge of improving their energy density remains crucial. Agglomeration of MXene nanosheets leads to irreversible capacity reduction, limiting their practical use. To tackle this issue, Xia *et al.* proposed an innovative solution: ionization-bombardment assisted deposition synthesis to create SiC/MXene heterostructures (Fig. 12b).[189] This method involved carbon and SiO$_2$ powders to high voltage, transforming them into SiC nanocrystals. These SiC nanocrystals were patterned into a mesoporous SiC nanomesh to increase the specific surface area, allowing for uniform deposition and self-assembly of MXene nanosheets. The resulting SiC/MXene heterostructure exhibits low barrier properties, fast electron migration rates, and strong bonding forces. The SiC nanomesh serves as a conductive network, supporting the MXene film, thereby increasing the ion storage space and allowing for an interconnected path of sodium ion conduction. The MXene/SiC MSC demonstrated a specific capacity of up to 97.8 m cm^{-2} at 1 A cm^{-2}.

Conductive polymers with pseudocapacitor behavior have gained significant attention due to their desirable properties.[193–195] However, poor cycling stability resulting from volume changes during the doping/dedoping redox process has limited their practical applications.[196–198] To address this challenge, Liu *et al.* designed electrodes with robust cycling capacity for supercapacitors (Fig. 12c).[56] They achieved this by coating conductive poly(3,4-ethylenedioxythiophene) (PEDOT) around free-standing SiC nanowires using an all-dry oxidative chemical vapor deposition (oCVD) method. The resulting SiC@PEDOT nanowire architecture exhibited a specific capacitance of 26.53 mF cm^{-2} at 0.2 mA cm^{-2}. Impressively, their aqueous-based supercapacitors demonstrated remarkable cycling stability, with 104% capacity retention after 10 000 cycles. This approach demonstrated the potential of SiC nanowires as scaffold materials for achieving outstanding energy storage performance.

The core-branch electrode material also can enhance the performance of SiC-based composite supercapacitors. Zhao *et al.* pioneered the integration of trim aligned Fe$_2$O$_3$ nanoneedle arrays with typical mesoporous structures and NiCo$_2$O$_4$/Ni(OH)$_2$ hybrid nanosheet arrays on SiC nanowire skeletons to create a novel freestanding core-branch negative and positive electrode material (Fig. 12d).[177] The unique electrode material demonstrates exceptional resistance to oxidation and corrosion, high conductivity, and a large-specific surface area. Leveraging these specially designed electrodes, the researchers developed a high-performance asymmetric supercapacitor (ASC) capable of achieving a maximum energy density of 103 W h kg^{-1} at a power density of 3.5 kW kg^{-1}. Even when the device is charged within 6.5 s, the energy density could still reach as high as 45 W h kg^{-1} at 26.1 kW kg^{-1}. Moreover, the ASC demonstrates a long cycling lifetime, with 86.6% capacitance retention even after 5000 cycles.

SiC-based composite materials, including SiC/C nanosheets, have demonstrated exceptional cycling stability and high specific areal capacitance. For example, Liu *et al.* successfully produced C-coated SiC nanosheets (SiC/C NSs) through wet-chemical etching,[69] yielding electrodes with excellent cycling stability and high specific areal capacitance. These electrodes showed a capacitance of 734 µF cm^{-2} at 10 mV s^{-1} and retained 86.6% of their capacitance after 20 000 cycles. These groundbreaking advancements in SiC-based composite supercapacitors underscore their enhanced durability and superior performance, promising a wide array of practical applications in energy storage technologies.
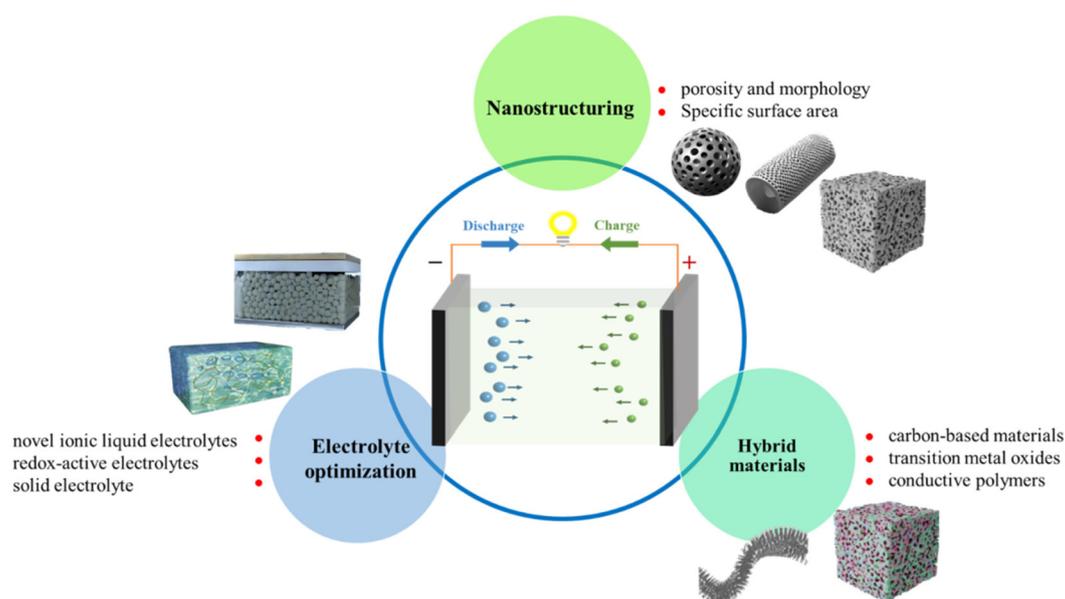

Fig. 13 The strategies for improving the performance of supercapacitors with SiC nanomaterials electrodes.

SiC-based composite materials offer numerous advantages, including high specific capacitance, excellent thermal stability, enhanced mechanical strength, a wide potential window, and good chemical compatibility. However, certain limitations, such as limited availability and high cost, complex fabrication processes, and relatively lower conductivity should be considered. To fully exploit the potential of SiC-based composite materials in supercapacitor applications, further research and development efforts are necessary to address these limitations and optimize their performance.

7 Conclusions and outlooks

SiC has garnered substantial attention in recent years due to its unique properties and potential as an electrode material in supercapacitors. However, there are certain limitations associated with the use of SiC as an electrode material in supercapacitors that must be addressed to fully harness its potential. (a) *Limited energy density*. One notable drawback of SiC-based supercapacitors is their relatively lower energy density when compared to other electrode materials, such as carbon-based materials. This limitation restricts their application in energy-intensive devices. (b) *Synthesis challenges*. The synthesis of SiC nanomaterials with controlled morphologies and well-defined structures can be a formidable task. These challenges in synthesis may impede large-scale production and integration into commercial supercapacitors.

To overcome these limitations and pave the way for future advancements, the following research directions should be considered (see Fig. 13). (a) *Nanostructuring techniques*. Innovative approaches for fabricating SiC nanomaterials with tailored properties, including controlled porosity and morphology, hold the potential to significantly enhance their energy storage capacity. (b) *Hybrid materials*: exploring the incorporation of SiC with other high-energy-density electrode materials, such as carbon-based materials or transition metal oxides, could potentially boost the overall energy density of supercapacitors. (c) *Electrolyte optimization*. Research efforts should be directed towards investigating advanced electrolyte systems that can enhance the charge storage mechanisms of SiC-based supercapacitors. The exploration of novel ionic liquid electrolytes or redox-active electrolytes may offer the prospect of achieving higher energy density and enabling higher voltage operation.

In conclusion, SiC nanomaterials exhibit substantial promise as electrodes in supercapacitors, boasting advantages such as a wide electrochemical stability window, superior mechanical strength, and remarkable resistance to extreme conditions. Nevertheless, addressing the challenges related to energy density and synthesis techniques is crucial. This can be achieved through the development of nanostructuring techniques, innovative hybrid material designs, and the optimization of electrolyte systems, ultimately unlocking the full potential of SiC in the construction of future supercapacitors.

Conflicts of interest

There are no conflicts of interest to declare.

Acknowledgements

References

1 J. Liang, C. Jiang and W. Wu, *Nanoscale*, 2019, **11**, 7041–7061.
2 J. H. Lee, G. Yang, C. H. Kim, R. L. Mahajan, S. Y. Lee and S. J. Park, *Energy Environ. Sci.*, 2022, **15**, 2233–2258.
3 M. Pershaanaa, S. Bashir, S. Ramesh and K. Ramesh, *J. Energy Storage*, 2022, **50**, 104599.
4 F. Naseri, S. Karimi, E. Farjah and E. Schaltz, *Renewable Sustainable Energy Rev.*, 2022, **155**, 111913.
5 J. Zhang, Y. Yan, X. Wang, Y. Cui, Z. Zhang, S. Wang, Z. Xie, P. Yan and W. Chen, *Nat. Commun.*, 2023, **14**, 3701.
6 Z. Wang, L. Wang, W. Jiang, X. Jian and F. Hu, *Sci. China Mater.*, 2023, **66**, 3129–3138.
7 J. Guo, Y. Liang, S. Zhang, D. Ma, T. Yang, W. Zhang, H. Li and S. Cao, *Green Energy Resour.*, 2023, **1**, 100007.
8 L. Huang, S. Cao, Y. Liang, J. Chen, T. Yang, J. Zhao and B. Zou, *J. Mater. Chem. C*, 2023, **11**, 10107–10120.
9 D. P. Chatterjee and A. K. Nandi, *J. Mater. Chem. A*, 2021, **9**, 15880–15918.
10 D. Chen, K. Jiang, T. Huang and G. Shen, *Adv. Mater.*, 2020, **32**, 1901806.
11 H. Zhang, Y. Cao, M. O. L. Chee, P. Dong, M. Ye and J. Shen, *Nanoscale*, 2019, **11**, 5807–5821.
12 H. Guentri, T. Allaoui, M. Mekki and M. Denai, *J. Energy Storage*, 2021, **39**, 102578.
13 J. R. Rajabathar, M. Sivachidambaram, J. J. Vijaya, H. A. Al-lohedan and D. M. D. Aldhayan, *ACS Omega*, 2020, **5**, 15028–15038.
14 L. Huang, S. Cao, J. Zhao and B. Zou, *J. Mater. Chem. C*, 2023, **11**, 10107–10120.
15 C. Meng, S. Knežević, F. Du, Y. Guan, F. Kanoufi, N. Sojic and G. Xu, *eScience*, 2022, **2**, 591–605.
16 F. Perez, G. Damm, C. M. Verrelli and P. F. Ribeiro, *IEEE Trans. Control Syst. Technol.*, 2023, **31**, 1552–1564.
17 D. Gutierrez-Rojas, P. H. J. Nardelli, G. Mendes and P. Popovski, *IEEE Trans. Industr. Inform.*, 2021, **17**, 1539–1552.
18 Z. Sun, X. Wen, L. Wang, D. Ji, X. Qin, J. Yu and S. Ramakrishna, *eScience*, 2022, **2**, 32–46.
19 X. Li, W. Ma, D. Liang, W. Cai, S. Zhao and Z. Zang, *eScience*, 2022, **2**, 646–654.

20 X. Zhang, R. Han, Y. Liu, H. Li, W. Shi, X. Yan, X. Zhao, Y. Li and B. Liu, *Chem. Eng. J.*, 2023, **460**, 141607.

21 C. Xiong, Q. Yang, W. Dang, Q. Zhou, X. Jiang, X. Sun, Z. Wang, M. An and Y. Ni, *J. Mater. Chem. A*, 2023, **11**, 4769–4779.

22 Y. Zhou, Y. Wang, K. Wang, L. Kang, F. Peng, L. Wang and J. Pang, *Appl. Energy*, 2020, **260**, 114169.

23 H. Li, A. Ravey, A. N'Diaye and A. Djerdir, *Energy Convers. Manage.*, 2019, **192**, 133–149.

24 Y. Wang, F. Chen, Z. Liu, Z. Tang, Q. Yang, Y. Zhao, S. Du, Q. Chen and C. Zhi, *Angew. Chem., Int. Ed.*, 2019, **58**, 15707–15711.

25 L. Yue, X. Wang, T. Sun, H. Liu, Q. Li, N. Wu, H. Guo and W. Yang, *Chem. Eng. J.*, 2019, **375**, 121959.

26 Y. Jiang and J. Liu, *Energy Environ. Sci.*, 2019, **2**, 30–37.

27 Y. Tao, Y. Wu, H. Chen, W. Chen, J. Wang, Y. Tong, G. Pei, Z. Shen and C. Guan, *Chem. Eng. J.*, 2020, **396**, 125364.

28 T. Yue, B. Shen and P. Gao, *Renewable Sustainable Energy Rev.*, 2022, **158**, 112131.

29 W. Li, X. Guo, K. Song, J. Chen, J. Zhang, G. Tang, C. Liu, W. Chen and C. Shen, *Adv. Energy Mater.*, 2023, **13**, 2300648.

30 S. Y. Attia, S. G. Mohamed, Y. F. Barakat, H. H. Hassan and W. A. Zoubi, *Rev. Inorg. Chem.*, 2022, **42**, 53–88.

31 B. Xu, H. Zhang, H. Mei and D. Sun, *Coord. Chem. Rev.*, 2020, **420**, 213438.

32 G. Nie, X. Zhao, Y. Luan, J. Jiang, Z. Kou and J. Wang, *Nanoscale*, 2020, **12**, 13225–13248.

33 S. Saini, P. Chand and A. Joshi, *J. Energy Storage*, 2021, **39**, 102646.

34 R. Kumar, E. Joanni, S. Sahoo, J. J. Shim, W. K. Tan, A. Matsuda and R. K. Singh, *Carbon*, 2022, **193**, 298–338.

35 D. G. Wang, Z. Liang, S. Gao, C. Qu and R. Zou, *Coord. Chem. Rev.*, 2020, **404**, 213093.

36 C. Jing, B. Dong and Y. Zhang, *Energy Environ. Sci.*, 2020, **3**, 346–379.

37 X. Chu, F. Meng, T. Deng and W. Zhang, *Nanoscale*, 2021, **13**, 5570–5593.

38 H. Zhuo, Y. Hu, Z. Chen and L. Zhong, *Carbohydr. Polym.*, 2019, **215**, 322–329.

39 Y. Wang, Y. Ding, X. Guo and G. Yu, *Nano Res.*, 2019, **12**, 1978–1987.

40 X. Sun, L. Li, S. Jin, W. Shao, H. Wang, X. Zhang and Y. Xie, *eScience*, 2023, **3**, 100095.

41 Z. Zhai, L. Zhang, T. Du, B. Ren, Y. Xu, S. Wang, J. Miao and Z. Liu, *Mater. Des.*, 2022, **221**, 111017.

42 J. Zhou, S. Zhang, Y. N. Zhou, W. Tang, J. Yang, C. Peng and Z. Guo, *Electrochem. Energy Rev.*, 2021, **4**, 219–248.

43 T. Huang, J. Ding, Z. Liu, R. Zhang, B. Zhang, K. Xiong, L. Zhang, C. Wang, S. Shen, C. Li, P. Yang and F. Qiu, *eScience*, 2022, **2**, 319–328.

44 J. Zhang, K. Zhan, S. Zhang, Y. Shen, Y. Hou, J. Liu, Y. Fan, Y. Zhang, S. Wang, Y. Xie, X. Chen and X. Hou, *eScience*, 2022, **2**, 615–622.

45 A. Nandagudi, S. H. Nagarajarao, M. S. Santosh, B. M. Basavaraja, S. J. Malode, R. J. Mascarenhas and N. P. Shetti, *Mater. Today Sustain.*, 2022, **19**, 100214.

46 N. S. Shaikh, S. B. Ubale, V. J. Mane, J. S. Shaikh, V. C. Lokhande, S. Praserthdam, C. D. Lokhande and P. Kanjanaboos, *J. Alloys Compd.*, 2022, **893**, 161998.

47 D. Tang, R. Yi, W. Zhang, Z. Qiao, Y. Liu, Q. Huo and D. Wang, *Mater. Lett.*, 2017, **198**, 140–143.

48 T. K. Nguyen, S. Aberoumand and D. V. Dao, *Small*, 2021, **17**, 2101775.

49 G. P. Ojha, G. W. Kang, Y. S. Kuk, Y. E. Hwang, O. H. Kwon, B. Pant, J. Acharya, Y. W. Park and M. Park, *Nanomaterials*, 2022, **13**, 150.

50 X. Li, W. Li, Q. Liu, S. Chen, L. Wang, F. Gao, G. Shao, Y. Tian, Z. Lin and W. Yang, *Adv. Funct. Mater.*, 2021, **31**, 2008901.

51 P. Kang, Q. Zhao, T. Zhang, W. Xue, J. Qian, Z. Wei, P. Wang and G. Wu, *J. Mater. Chem. A*, 2023, **11**, 15347–15358.

52 X. Li, Q. Liu, S. Chen, W. Li, Z. Liang, Z. Fang, W. Yang, Y. Tian and Y. Yang, *Energy Storage Mater.*, 2020, **27**, 261–269.

53 W. Li, Q. Liu, Z. Fang, L. Wang, S. Chen, F. Gao, Y. Ji, W. Yang and X. Fang, *Adv. Energy Mater.*, 2019, **9**, 1900073.

54 X. Tang, Z. Hu, Z. Wang, J. Chen, X. Mu, G. Song, P. Sun, Z. Wen, J. Hao, S. Cong and Z. Zhao, *eScience*, 2022, **2**, 632–638.

55 J. Zhao, Z. Li, M. Zhang, A. Meng and Q. Li, *ACS Sustainable Chem. Eng.*, 2016, **4**, 3598–3608.

56 W. Liu, X. Li, W. Li, Y. Ye, H. Wang, P. Su, W. Yang and Y. Yang, *J. Energy Chem.*, 2022, **66**, 30–37.

57 X. Yin, H. Li, L. Han, R. Yuan and J. Lu, *J. Colloid Interface Sci.*, 2020, **577**, 481–493.

58 X. She, A. Q. Huang, Ó. Lucía and B. Ozpineci, *IEEE Trans. Ind. Appl.*, 2017, **64**, 8193–8205.

59 J. Wei, Z. Wei, H. Fu, J. Cao, T. Wu, J. Sun, X. Zhu, S. Li, L. Zhang, S. Liu and W. Sun, *IEEE Trans. Power Electron.*, 2023, **38**, 8990–9005.

60 H. S. Kim and Y. W. Kim, *J. Eur. Ceram. Soc.*, 2023, **43**, 3855–3874.

61 R. Wu, K. Zhou, C. Y. Yue, J. Wei and Y. Pan, *Prog. Mater. Sci.*, 2015, **72**, 1–60.

62 R. He, N. Zhou, K. Zhang, X. Zhang, L. Zhang, W. Wang and D. Fang, *J. Adv. Ceram.*, 2021, **10**, 637–674.

63 G. Tuci, Y. Liu, A. Rossin, X. Guo, C. Pham, G. Giambastiani and C. Pham-Huu, *Chem. Rev.*, 2021, **121**, 10559–10665.

64 C. H. Chang, B. Hsia, J. P. Alper, S. Wang, L. E. Luna, C. Carraro, S. Y. Lu and R. Maboudian, *ACS Appl. Mater. Interfaces*, 2015, **7**, 26658–26665.

65 S. Chen, W. Li, X. Li and W. Yang, *Prog. Mater. Sci.*, 2019, **104**, 138–214.

66 P. J. Wellmann, M. Arzig, J. Ihle, M. Kollmuss, J. Steiner, M. Mauceri, D. Crippa, F. La Via, M. Salamon, N. Uhlmann, M. Roder, A. N. Danilewsky, B. D. Nguyen and S. Sandfeld, *Mater. Sci. Forum*, 2022, **1062**, 104–112.

67 Q. Q. Shao and H. Gu, *J. Materiomics*, 2023, **9**, 299–309.

68 M. Gao, W. K. Wang, Q. Rong, J. Jiang, Y. J. Zhang and H. Q. Yu, *ACS Appl. Mater. Interfaces*, 2018, **10**, 23163–23173.

69 S. Liu, E. Wang, S. Liu, C. Guo, H. Wang, T. Yang and X. Hou, *J. Mater. Sci. Technol.*, 2022, **110**, 178–186.

70 N. H. D. Azevedo, P. R. de Matos, P. J. P. Gleize and A. M. Betioli, *Cem. Concr. Compos.*, 2021, **117**, 103903.

71 M. Xu, Y. R. Girish, K. P. Rakesh, P. Wu, H. M. Manukumar, S. M. Byrappa, Udayabhanu and K. Byrappa, *Mater. Today Commun.*, 2021, **28**, 102533.

72 C. L. Zhang and S. H. Yu, *Chem. Soc. Rev.*, 2014, **43**, 4423–4448.

73 J. Xue, T. Wu, Y. Dai and Y. Xia, *Chem. Rev.*, 2019, **119**, 5298–5415.

74 Q. Liu, J. Zhu, L. Zhang and Y. Qiu, *Renewable Sustainable Energy Rev.*, 2018, **81**, 1825–1858.

75 Y. Liao, C. H. Loh, M. Tian, R. Wang and A. G. Fane, *Prog. Polym. Sci.*, 2018, **77**, 69–94.

76 Y. Li, J. Zhu, H. Cheng, G. Li, H. Cho, M. Jiang, Q. Gao and X. Zhang, *Adv. Mater. Technol.*, 2021, **6**, 2100410.

77 D. G. Shin, D. H. Riu and H. E. Kim, *J. Ceram. Process. Res.*, 2008, **9**, 209–214.

78 Y. Liu, H. Hou, X. He and W. Yang, *Sci. Rep.*, 2017, **7**, 1893.

79 B. Wang, L. Sun, N. Wu and Y. Wang, *Ceram. Int.*, 2017, **43**, 10619–10623.

80 H. A. Liu and K. J. Balkus, *Mater. Lett.*, 2009, **63**, 2361–2364.

81 H. Hou, F. Gao, G. Wei, M. Wang, J. Zheng, B. Tang and W. Yang, *Cryst. Growth Des.*, 2012, **12**, 536–539.

82 P. Wang, L. Cheng, Y. Zhang and L. Zhang, *J. Alloys Compd.*, 2017, **716**, 306–320.

83 H. Guo, Y. Chen, Y. Li, W. Zhou, W. Xu, L. Pang, X. Fan and S. Jiang, *Composites, Part A*, 2021, **143**, 106309.

84 S. H. Choi, D. Y. Youn, S. M. Jo, S. G. Oh and I.-D. Kim, *ACS Appl. Mater. Interfaces*, 2011, **3**, 1385–1389.

85 F. E. Ahmed, B. S. Lalia and R. Hashaikeh, *Desalination*, 2015, **356**, 15–30.

86 B. Yao, B. Lu, Q. Huang, Z. R. Huang and Q. Yuan, *Ceram. Int.*, 2020, **46**, 9894–9900.

87 B. Sun, Y. Z. Long, H. D. Zhang, M. M. Li, J. L. Duvail, X. Y. Jiang and H. L. Yin, *Prog. Polym. Sci.*, 2014, **39**, 862–890.

88 J. Wei, X. Li, Y. Wang, B. Chen, M. Zhang and C. Qin, *J. Am. Ceram. Soc.*, 2020, **103**, 6187–6197.

89 S. J. Kim, S. M. Yun and Y. S. Lee, *J. Ind. Eng. Chem.*, 2010, **16**, 273–277.

90 D. Bokov, A. Turki Jalil, S. Chupradit, W. Suksatan, M. Javed Ansari, I. H. Shewael, G. H. Valiev and E. Kianfar, *Adv. Mater. Sci. Eng.*, 2021, **2021**, 5102014.

91 Z. Omidi, A. Ghasemi and S. R. Bakhshi, *Ceram. Int.*, 2015, **41**, 5779–5784.

92 J. Li, J. Tian and L. Dong, *J. Eur. Ceram. Soc.*, 2000, **20**, 1853–1857.

93 O. Kettner, S. Šimić, B. Kunert, R. Schennach, R. Resel, T. Grießer and B. Friedel, *Adv. Eng. Mater.*, 2018, **20**, 1701067.

94 P. Gupta, W. Wang and L. S. Fan, *Ind. Eng. Chem. Res.*, 2004, **43**, 4732–4739.

95 K. C. Hung, T. L. Wu, J. W. Xu and J. H. Wu, *Polymers*, 2019, **11**, 1442.

96 F. Li, L. Zhou, J.-X. Liu and G.-J. Zhang, *Materials*, 2023, **16**, 220.

97 A. Feinle, M. S. Elsaesser and N. Hüsing, *Chem. Soc. Rev.*, 2016, **45**, 3377–3399.

98 G. Q. Jin and X. Y. Guo, *Microporous Mesoporous Mater.*, 2003, **60**, 207–212.

99 G. Q. Jin, P. Liang and X. Y. Guo, *J. Mater. Sci. Lett.*, 2003, **22**, 767–770.

100 Y. Kong, X. Shen, S. Cui and M. Fan, *Ceram. Int.*, 2014, **40**, 8265–8271.

101 L. Li, X. Liu, G. Wang, Y. Liu, W. Kang, N. Deng, X. Zhuang and X. Zhou, *Chem. Eng. J.*, 2021, **421**, 127744.

102 S. M. Attia, J. Wang, G. M. Wu, J. Shen and J. H. Ma, *J. Mater. Sci. Technol.*, 2002, **18**, 211–218.

103 Z. Li, J. Zhang, A. Meng and J. Guo, *J. Phys. Chem. B*, 2006, **110**, 22382–22386.

104 J. Zhou, B. Wei, Z. Yao, H. Lin, R. Tan, W. Chen and X. Guo, *J. Alloys Compd.*, 2020, **819**, 153021.

105 Z. Liu, W. Shen, W. Bu, H. Chen, Z. Hua, L. Zhang, L. Li, J. Shi and S. Tan, *Microporous Mesoporous Mater.*, 2005, **82**, 137–145.

106 Q. Qin, J. Chen, M. Song, F. Cao, Y. Li, F. He, Z. Liu, G. Zhu and Q. Diao, *J. Alloys Compd.*, 2022, **910**, 164746.

107 J. Wang, L. Wang, J. Diao, X. Xie, G. Lin, Q. Jia, H. Liu and G. Sui, *J. Mater. Sci. Technol.*, 2022, **103**, 209–214.

108 J. W. Kim, S. W. Myoung, H. C. Kim, J. H. Lee, Y. G. Jung and C. Y. Jo, *Mater. Sci. Eng., A*, 2006, **434**, 171–177.

109 Y. F. Shi, Y. Meng, D. H. Chen, S. J. Cheng, P. Chen, H. F. Yang, Y. Wan and D. Y. Zhao, *Adv. Funct. Mater.*, 2006, **16**, 561–567.

110 D. Xu, C. Zhen and H. Zhao, *Ceram. Int.*, 2020, **46**, 19629–19633.

111 Y. Shi, F. Zhang, Y. S. Hu, X. Sun, Y. Zhang, H. I. Lee, L. Chen and G. D. Stucky, *J. Am. Chem. Soc.*, 2010, **132**, 5552–5553.

112 X. F. Zhang, Z. Chen, Y. Feng, J. Qiu and J. Yao, *ACS Sustainable Chem. Eng.*, 2018, **6**, 1068–1073.

113 J. Ahn, H. S. Kim, J. Pyo, J. K. Lee and W. C. Yoo, *Chem. Mater.*, 2016, **28**, 1526–1536.

114 Y. Wang, L. Zhang, X. Zhang, Z. Zhang, Y. Tong, F. Li, J. C. S. Wu and X. Wang, *Appl. Catal., B*, 2017, **206**, 158–167.

115 Y. Wan, H. Yang and D. Zhao, *Acc. Chem. Res.*, 2006, **39**, 423–432.

116 L. M. Rueschhoff, L. A. Baldwin, R. Wheeler, M. J. Dalton, H. Koerner, J. D. Berrigan, N. M. Bedford, S. Seifert, M. K. Cinibulk and M. B. Dickerson, *ACS Appl. Nano Mater.*, 2019, **2**, 250–257.

117 P. C. Gao, P. Simon and F. Favier, *Microporous Mesoporous Mater.*, 2013, **180**, 172–177.

118 K. Chen, Z. Huang, J. Huang, M. Fang, Y. G. Liu, H. Ji and L. Yin, *Ceram. Int.*, 2013, **39**, 1957–1962.

119 D. Chen, Z. Liu, B. Liang, X. Wang and G. Shen, *Nanoscale*, 2012, **4**, 3001–3012.

120 W. Lin, L. Chengming, Y. Yang, C. Shanliang, G. Fengmei, W. Guodong and Y. Weiyou, *ACS Appl. Mater. Interfaces*, 2015, **7**, 526–533.

121 H. Wang, Z. Xie, W. Yang, J. Fang and L. An, *Cryst. Growth Des.*, 2008, **8**, 3893–3896.

122 S. Chen, P. Ying, L. Wang, G. Wei, F. Gao, J. Zheng, M. Shang, Z. Yang, W. Yang and T. Wu, *NPG Asia Mater.*, 2015, **7**, 157.

123 L. Wang, F. Gao, S. Chen, C. Li and W. Yang, *Appl. Phys. Lett.*, 2015, **107**, 122108.

124 Y. Sun, H. Cui, G. Z. Yang, H. Huang, D. Jiang and C. X. Wang, *CrystEngComm*, 2010, **12**, 1134–1138.

125 S. Chen, P. Ying, L. Wang, F. Gao, G. Wei, J. Zheng, Z. Xie and W. Yang, *RSC Adv.*, 2014, **4**, 8376–8382.

126 H. Wang, Z. Xie, W. Yang, J. Fang and L. An, *Cryst. Growth Des.*, 2008, **8**, 3893–3896.

127 C. H. Wang, H. K. Lin, T. Y. Ke, T. J. Palathinkal, N. H. Tai, I. N. Lin, C. Y. Lee and H. T. Chiu, *Chem. Mater.*, 2007, **19**, 3956–3962.

128 R. Ren, D. Xiang, Y. Cao and Y. Hu, *J. Alloys Compd.*, 2021, **857**, 157577.

129 H. Li, Q. Dong, X. Zheng, J. Chen, Y. Lou, J. Yang, M. Zhu, L. Lv, H. Zhu, X. Yang and Q. Shan, *ACS Sustainable Chem. Eng.*, 2023, **11**, 2554–2563.

130 J. Chen, Q. Shi, L. Xin, Y. Liu, R. Liu and X. Zhu, *J. Alloys Compd.*, 2011, **509**, 6844–6847.

131 K. B. Tang, Y. T. Qian, J. H. Zeng and X. G. Yang, *Adv. Mater.*, 2003, **15**, 448–450.

132 Z. Ju, X. Ma, N. Fan, P. Li, L. Xu and Y. Qian, *Mater. Lett.*, 2007, **61**, 3913–3915.

133 X. L. Wu, J. Y. Fan, T. Qiu, X. Yang, G. G. Siu and P. K. Chu, *Phys. Rev. Lett.*, 2005, **94**, 026102.

134 E. J. Connolly, B. Timmer, H. T. M. Pham, J. Groeneweg, P. M. Sarro, W. Olthuis and P. J. French, *Sens. Actuators, B*, 2005, **109**, 44–46.

135 G. Zou, C. Dong, K. Xiong, H. Li, C. Jiang and Y. Qian, *Appl. Phys. Lett.*, 2006, **88**, 7.

136 G. Shen, D. Chen, K. Tang, Y. Qian and S. Zhang, *Chem. Phys. Lett.*, 2003, **375**, 177–184.

137 Q. Lu, J. Hu, K. Tang, Y. Qian, G. Zhou, X. Liu and J. Zhu, *Appl. Phys. Lett.*, 1999, **75**, 507–509.

138 M. Zhang, *J. Phys. Chem. Solids*, 2017, **103**, 1–5.

139 D. Zhuang and J. H. Edgar, *Mater. Sci. Eng., R*, 2005, **48**, 1–46.

140 J. Y. Fan, X. L. Wu and P. K. Chu, *Prog. Mater. Sci.*, 2006, **51**, 983–1031.

141 D. H. van Dorp, J. J. H. B. Sattler, J. H. den Otter and J. J. Kelly, *Electrochim. Acta*, 2009, **54**, 6269–6275.

142 S. Xu, F. Jiang, F. Gao, L. Wang, J. Teng, D. Fu, H. Zhang, W. Yang and S. Chen, *ACS Appl. Mater. Interfaces*, 2020, **12**, 20469–20478.

143 L. Zhao, S. Chen, L. Wang, F. Gao, X. Yao and W. Yang, *Ceram. Int.*, 2018, **44**, 7280–7285.

144 M. I. A. Abdel Maksoud, R. A. Fahim, A. E. Shalan, M. Abd Elkodous, S. O. Olojede, A. I. Osman, C. Farrell, A. a. H. Al-Muhtaseb, A. S. Awed, A. H. Ashour and D. W. Rooney, *Environ. Chem. Lett.*, 2021, **19**, 375–439.

145 R. E. Ustad, S. S. Kundale, K. A. Rokade, S. L. Patil, V. D. Chavan, K. D. Kadam, H. S. Patil, S. P. Patil, R. K. Kamat, D. k. Kim and T. D. Dongale, *Nanoscale*, 2023, **15**, 9891–9926.

146 T. Li, T. Qin, C. Yang, W. Zhang and W. Zhang, *Nanoscale*, 2021, **13**, 3412–3435.

147 P. Naskar, A. Maiti, P. Chakraborty, D. Kundu, B. Biswas and A. Banerjee, *J. Mater. Chem. A*, 2021, **9**, 1970–2017.

148 W. Dong, M. Xie, S. Zhao, Q. Qin and F. Huang, *Mater. Sci. Eng., R*, 2023, **152**, 100713.

149 Z. Yang, J. Tian, Z. Ye, C. Jin, C. Cui, Q. Xie, J. Wang, G. Zhang, Z. Dong, Y. Miao, X. Yu, W. Qian and F. Wei, *Energy Storage Mater.*, 2020, **33**, 18–25.

150 K. Krishnamoorthy, P. Pazhamalai, V. K. Mariappan, S. S. Nardekar, S. Sahoo and S. J. Kim, *Nat. Commun.*, 2020, **11**, 2351.

151 P. Merin, P. Jimmy Joy, M. N. Muralidharan, E. Veena Gopalan and A. Seema, *Chem. Eng. Technol.*, 2021, **44**, 844–851.

152 B. Zhao, D. Chen, X. Xiong, B. Song, R. Hu, Q. Zhang, B. H. Rainwater, G. H. Waller, D. Zhen, Y. Ding, Y. Chen, C. Qu, D. Dang, C. P. Wong and M. Liu, *Energy Storage Mater.*, 2017, **7**, 32–39.

153 M. Tahir, L. He, W. A. Haider, W. Yang, X. Hong, Y. Guo, X. Pan, H. Tang, Y. Li and L. Mai, *Nanoscale*, 2019, **11**, 7761–7770.

154 Y. Deng, H. Wang, K. Zhang, J. Shao, J. Qiu, J. Wu, Y. Wu and L. Yan, *Nanoscale*, 2021, **13**, 3010–3018.

155 J. Xu, R. Jin, X. Ren and G. Gao, *Chem. Eng. J.*, 2021, **413**, 127446.

156 S. Yu, J. Chen, C. Chen, M. Zhou, L. Shen, B. Li and H. Lin, *Coord. Chem. Rev.*, 2023, **482**, 215082.

157 L. Gu, Y. Wang, Y. Fang, R. Lu and J. Sha, *J. Power Sources*, 2013, **243**, 648–653.

158 J. P. Alper, M. S. Kim, M. Vincent, B. Hsia, V. Radmilovic, C. Carraro and R. Maboudian, *J. Power Sources*, 2013, **230**, 298–302.

159 Y. Chen, X. Zhang and Z. Xie, *ACS Nano*, 2015, **9**, 8054–8063.

160 L. Gu, Y. Wang, R. Lu, W. Wang, X. Peng and J. Sha, *J. Power Sources*, 2015, **273**, 479–485.

161 M. Kim, I. Oh and J. Kim, *J. Mater. Chem. A*, 2015, **3**, 3944–3951.

162 Y. Zhao, W. Kang, L. Li, G. Yan, X. Wang, X. Zhuang and B. Cheng, *Electrochim. Acta*, 2016, **207**, 257–265.

163 M. Kim, I. Oh and J. Kim, *Chem. Eng. J.*, 2016, **289**, 170–179.

164 A. Sanger, A. Kumar, A. Kumar, P. K. Jain, Y. K. Mishra and R. Chandra, *Ind. Eng. Chem. Res.*, 2016, **55**, 9452–9458.

165 W. Li, Q. Liu, S. Chen, Z. Fang, X. Liang, G. Wei, L. Wang, W. Yang, Y. Ji and L. Mai, *Mater. Horiz.*, 2018, **5**, 883–889.

166 Q. Sun, R. Tu, Q. Xu, C. Zhang, J. Li, H. Ohmori, M. Kosinova, B. Basu, J. Yan, S. Li, T. Goto, L. Zhang and S. Zhang, *J. Power Sources*, 2019, **444**, 227308.

167 J. Liang, J. Lu, P. Gao, W. Guo and H. Xiao, *J. Alloys Compd.*, 2020, **827**, 154168.

168 X. Liu, H. Zhao, S. Jiang, S. Wu, T. Zhao, L. Li, X. Geng, H. Yang, W. Zhou, C. Sun, Y. Chen and B. An, *J. Alloys Compd.*, 2021, **881**, 160442.

169 Z. Zhang, J. Tan, L. Cheng and W. Yang, *Ceram. Int.*, 2021, **47**, 24652–24662.

170 S. Xie, X. N. Guo, G.-Q. Jin, X. L. Tong, Y. Y. Wang and X. Y. Guo, *Chem. Commun.*, 2014, **50**, 228–230.

171 M. Kim, Y. Yoo and J. Kim, *J. Power Sources*, 2014, **265**, 214–222.

172 M. Kim and J. Kim, *ACS Appl. Mater. Interfaces*, 2014, **6**, 9036–9045.

173 Y. Zhang, J. Chen, H. Fan, K. C. Chou and X. Hou, *Dalton Trans.*, 2015, **44**, 19974–19982.

174 J. Zhao, Z. Li, M. Zhang, A. Meng and Q. Li, *J. Power Sources*, 2016, **332**, 355–365.

175 N. b. Hamzan, M. M. b. Ramly, N. M. Huang, S. A. Rahman and B. T. Goh, *Mater. Charact.*, 2017, **132**, 187–198.

176 M. Kim, J. Yoo and J. Kim, *Chem. Eng. J.*, 2017, **324**, 93–103.

177 J. Zhao, Z. Li, X. Yuan, Z. Yang, M. Zhang, A. Meng and Q. Li, *Adv. Energy Mater.*, 2018, **8**, 1702787.

178 M. Zeraati and K. Tahmasebi, *J. Alloys Compd.*, 2019, **786**, 798–807.

179 J. Zhao, Z. Li, X. Yuan, T. Shen, L. Lin, M. Zhang, A. Meng and Q. Li, *Chem. Eng. J.*, 2019, **357**, 21–32.

180 K. Kundu, A. Ghosh, A. Ray, S. Das, J. Chakraborty, S. Kumar, N. E. Prasad and R. Banerjee, *J. Mater. Sci.: Mater. Electron.*, 2020, **31**, 17943–17952.

181 N. b. Hamzan, M. M. b. Ramly, M. F. b. Omar, H. Nakajima, S. Tunmee, S. A. Rahman and B. T. Goh, *Thin Solid Films*, 2020, **716**, 138430.

182 Q. Tang, X. Chen, D. Zhou and C. Liu, *Colloids Surf., A*, 2021, **620**, 126567.

183 C. P. Lee, B. T. Murti, P. K. Yang, F. Rossi, C. Carraro and R. Maboudian, *Materials*, 2021, **14**, 4514.

184 M. Zeraati, V. Alizadeh, G. Sargazi and H. Kazemian, *J. Mater. Sci.: Mater. Electron.*, 2021, **32**, 22319–22329.

185 X. Yin, H. Li, R. Yuan and J. Lu, *J. Colloid Interface Sci.*, 2021, **586**, 219–232.

186 X. Yin, H. Li, R. Yuan and J. Lu, *J. Mater. Sci. Technol.*, 2021, **81**, 162–174.

187 R. Wang, W. Li, L. Jiang, Q. Liu, L. Wang, B. Tang and W. Yang, *Electrochim. Acta*, 2022, **406**, 139867.

188 K. Zhu, M. Li, C. Li, X. Xuan and H. Li, *Chem. Eng. J.*, 2022, **433**, 133576.

189 M. Xia, J. Ning, X. Feng, H. Guo, D. Wang, J. Zhang and Y. Hao, *Chem. Eng. J.*, 2022, **428**, 131114.

190 X. Li, J. Chen, S. Chen, W. Li, J. Yang, F. Hu, Q. Wei, X. Zhao, X. Zhang and W. Yang, *J. Mater. Chem. A*, 2022, **10**, 15708–15718.

191 S. C. Abbas, C. Lin, Z. Hua, Q. Deng, H. Huang, Y. Ni, S. Cao and X. Ma, *Chem. Eng. J.*, 2022, **433**, 133738.

192 M. Bayona Becerra, J. Aceros Cabezas, V. Güiza Argüello and S. Blanco, *MRS Commun.*, 2023, **13**, 240–247.

193 Y. Yao, N. Liu, M. T. McDowell, M. Pasta and Y. Cui, *Energy Environ. Sci.*, 2012, **5**, 7927–7930.

194 F. Niu, R. Guo, L. Dang, J. Sun, Q. Li, X. He, Z. Liu and Z. Lei, *ACS Appl. Energy Mater.*, 2020, **3**, 7794–7803.

195 D. Gan, Z. Huang, X. Wang, D. Xu, S. Rao, K. Wang, F. Ren, L. Jiang, C. Xie and X. Lu, *Mater. Horiz.*, 2023, **10**, 2169–2180.

196 Y. Zhou, N. Lachman, M. Ghaffari, H. Xu, D. Bhattacharya, P. Fattahi, M. R. Abidian, S. Wu, K. K. Gleason, B. L. Wardle and Q. M. Zhang, *J. Mater. Chem. A*, 2014, **2**, 9964–9969.

197 S. Fleischmann, J. B. Mitchell, R. Wang, C. Zhan, D. E. Jiang, V. Presser and V. Augustyn, *Chem. Rev.*, 2020, **120**, 6738–6782.

198 B. Huang, Z. Sun and G. Sun, *eScience*, 2022, **2**, 243–277.